BILINGUAL PUBLISHING GROUP

Journal of Building Material Science

Volume 5 • Issue 2 • December 2023 ISSN 2630-5216(Online)

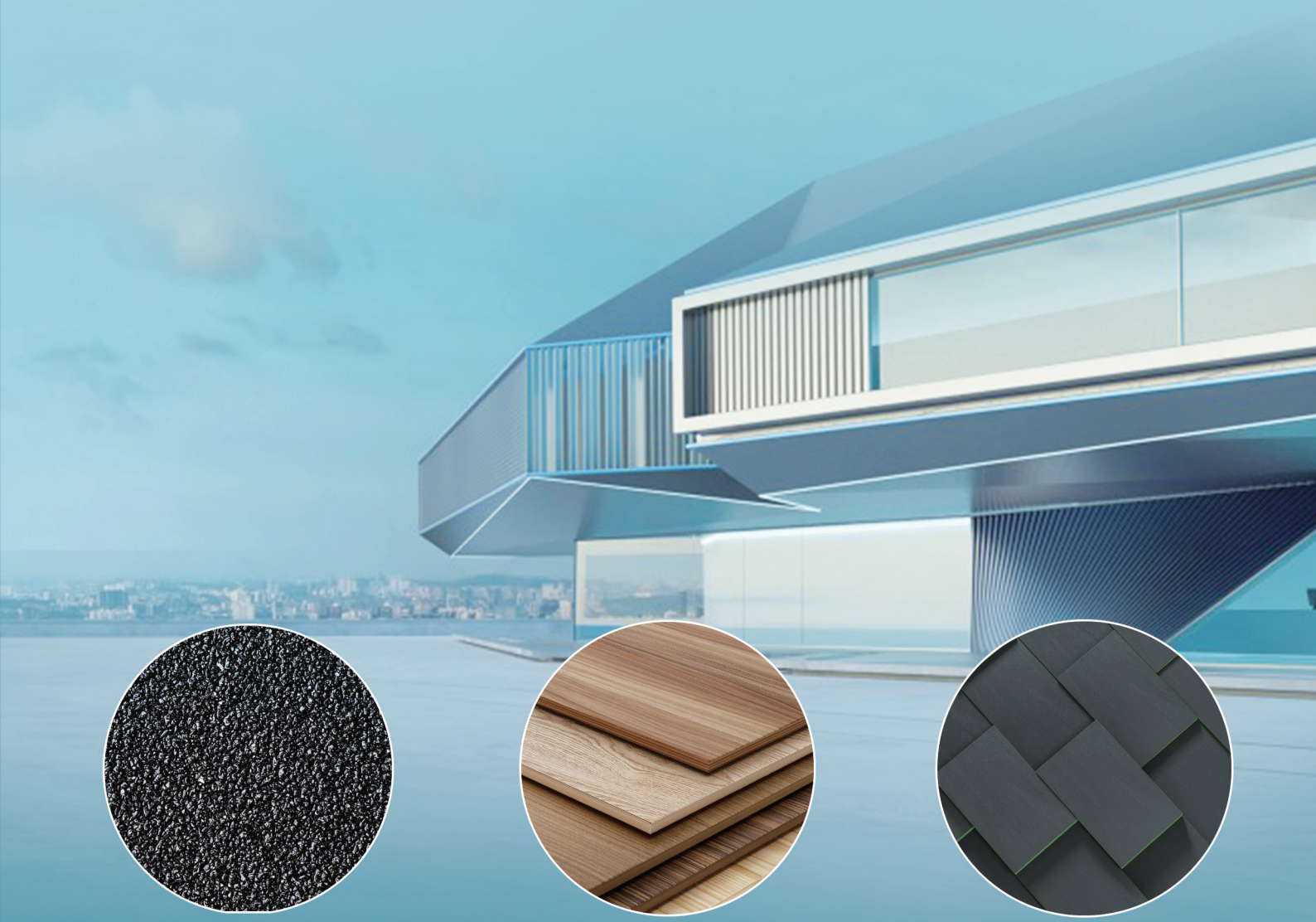

BILINGUAL PUBLISHING GROUP

Editor-in-Chief

Dr. Zhibin Lin

North Dakota State University, United States

Dr. Subhadip Mondal

Jeonbuk National University, South Korea

Associate Editors

Dr. Ying Huang

North Dakota State University, United States

Dr. Haradhan Kolya

Jeonbuk National University, Republic of Korea

Editorial Board Members

Prof. Dr. Bin Xu	Huaqiao University, China
Prof. Dr. Luigi Coppola	University of Bergamo, Italy
Prof. Dr. Xiaoshu Lu	University of Vaasa, Finland
Dr. Hosam M. Saleh	Egyptian Atomic Energy Authority, Egypt
Dr. Meng Guo	Beijing University of Technology, China
Dr. Sudarshan Dattatraya Kore	NICMAR University, Pune, India
Dr. Mohammad Jamshidi Avanaki	International University of Chabahar, Iran
Dr. Kiran Devi	SGT University, Gurugram, India
Dr. Jacopo Donnini	Marche Polytechnic University, Italy
Dr. Susana Hormigos-Jimenez	San Pablo CEU University, Spain
Dr. Santiranjan Shannigrahi	Institute of Materials Research and Engineering (ASTAR), Singapore
Dr. Ahmed S. H. Suwaed	Heriot-Watt University, United Kingdom
Dr. Leila Soufeiani	University of Melbourne, Australia

Volume 5 Issue 2 • December 2023 • ISSN 2630-5216 (Online)

JOURNAL OF BUILDING MATERIAL SCIENCE

Editor-in-Chief

Dr. Zhibin Lin

Dr. Subhadip Mondal

BILINGUAL PUBLISHING GROUP

BILINGUAL PUBLISHING GROUP

Volume 5 | Issue 2 | December 2023 | Page1-59

Journal of Building Material Science

Contents

Articles

Review

BILINGUAL PUBLISHING GROUP

Journal of Building Material Science

https://journals.bilpubgroup.com/index.php/jbms

ARTICLE

Characteristics of Rice Husk-Admixed Conplast SP 430 Concrete

***Augustine Uchechukwu Elinwa*[1*], *Johnson Olomi Olakunle*[2]**

[1] *Civil Engineering Department, Abubakar Tafawa Balewa University, Bauchi, Bauchi State, 740001, Nigeria*

[2] *Works Department, University of Jos Teaching Hospital, Jos, Plateau State, 930211, Nigeria*

ABSTRACT

Experimental work was mounted using 5.7 mL of the Conplast SP430 admixture and rice husk ash (RHA) at replacement levels of 0 to 50% at 10% intervals by wt. % of cement. It is on the performance of Conplast SP 430 admixture and its effects on concrete and concrete with rice husk ash. Concrete specimens were cast and cured for 3 to 90 days and subjected to slump and mechanical characteristics tests. Data generated from the experiments were analyzed and sensitivity analysis of the concrete mix was determined using the Minitab 18 Statistical Package. The results showed that CP with concrete improves the workability of the concrete and reduces water absorption. The reverse was the case when RHA was used with the admixture which may be an issue of compatibility. The statistical characteristics restrict good and within the specified limits.

Keywords: Rice husk ash; Admixture; Mechanical characteristics; Statistical analysis

1. Introduction

The construction concrete industry is one of the largest sources of greenhouse gas (GHG) emissions with a magnitude of 50% of the world's emissions [1]. Portland cement (PC) is one of the most important concrete parameters that contribute significantly to GHG [2]. Its manufacture contributes to global CO_2 emissions approximately 7% of the total emissions. The calcination of CaO in the production of cement contributes approximately 50% of the GHG emissions.

Today, a great number of agricultural wastes are used as cement replacement materials (CRMs) or supplementary cement materials (SCMs) and it is one such strategy that has resulted in a large decrease

*CORRESPONDING AUTHOR:
Augustine Uchechukwu Elinwa, Civil Engineering Department, Abubakar Tafawa Balewa University, Bauchi, Bauchi State, 740001, Nigeria; Email: auelinwa@gmail.com

ARTICLE INFO
Received: 19 April 2023 | Revised: 11 May 2023 | Accepted: 25 June 2023 | Published Online: 3 July 2023
DOI: https://doi.org/10.30564/jbms.v5i2.5664

CITATION
Elinwa, A.U., Olakunle, J.O., 2023. Characteristics of Rice Husk-Admixed Conplast SP 430 Concrete. Journal of Building Material Science. 5(2): 1-14. DOI: https://doi.org/10.30564/jbms.v5i2.5664

COPYRIGHT
Copyright © 2023 by the author(s). Published by Bilingual Publishing Group. This is an open access article under the Creative Commons Attribution-NonCommercial 4.0 International (CC BY-NC 4.0) License. (https://creativecommons.org/licenses/by-nc/4.0/).

in the use of traditional Portland cement while also removing the hazards associated with the disposal of waste materials from diverse industries [3]. Recent sustainable research in concrete shows that the most effective strategy to lower the carbon footprint in the building sector is to substitute acceptable alternative cementitious materials for PC clinker [4]. Rice husk, a byproduct from rice processing has been used for concrete production based on the high percentage of the silicate content which is very high. The use of the material is by calcination of the husk to a temperature range of 400-600 °C. This produces ash of acceptable quality for concrete production [5].

Experimental data collected from these agricultural byproducts are subjected to variable factors ranging from an environment where they are grown to the prevailing climate. These are some of the reasons for data variabilities. RHA has been identified as a porous material with a large specific surface, and angular structure which can significantly affect the water demand [6,7]. Superplasticizers (SP) are widely used in concrete to limit water demand while improving the workability and maintaining or improving the strength of the concrete [7].

Conplast SP 430 admixture is used as the SP in this work. This use of Conplast SP 430 with RHA for concrete has not received wide publicity in the literature. The characteristics of the SP are shown in **Tables 1-3**. This superplasticizer conforms to ASTM-C-494-92 [8], chloride-free which is based on the selected sulfonated naphthalene polymers. It is a brown solution that disperses in water and is suitable for use with all types of Portland cement and cement replacement materials such as rice husk ash [9].

The performance of the product identified in **Table 2** is in conformity with the set of declared performance. This declaration of performance is issued in accordance with Regulation (EU) No 305/2011, under the sole responsibility of the manufacturer [9].

The thrust of this work, therefore, is an evaluation performance of CP as an admixture material and its possible effects on concrete and RHA-concrete. The acceptability of the experimental data on workability, water absorption, density, and the compressive strengths of RHA and RHA-CP concrete samples were confirmed using established statistical methods in Minitab 18 Software. These statistical measures include mean ($\bar{x}$), standard deviation (s), coefficient of determination (r^2), coefficient of variation (CoV), and performance index (ρ).

Table 1. Typical properties of Conplast SP 430.

Parameter	Description
Appearance	Brown liquid
Specific gravity	1.18 @ 25 °C
Chloride content	Nil to BS 5075/BS: EN934
Air entrainment	Less than 2% additional air is entrained at normal dosages

Table 2. Essential characteristics of Conplast SP 430.

Essential characteristics	Performance	Test method
Chloride ion content	≤ 0.1% by mass	EN934-2:2009
Alkali content	≤ 7.2 by mass	EN934-2:2009
Corrosion behavior	Contains only compounds according to EN 931-1-2008	EN934-2:2009
Water reduction	Test mix 12% with control	EN934-2:2009
Increase in consistence	Increase in slump ≥ 120 mm from initial (30 10 mm) Increase in flow ≥ 160 mm from initial (350 ± 20 mm)	EN934-2:2009
Retention of consistence	In 30 min after the addition, that mix value	EN934-2:2009
Compressive strength-equal consistence	At 1 day, test mix ≥ 140% of control mix. At 28 days, test mix ≥ 115% of control mix.	EN934-2:2009
Compressive strength-equal W/C ratio	At 28 days, test mix ≥ 90% of control mix. Test mix ≤ 2	EN934-2:2009
Dangerous substance	NPD (No Performance Declared)	
Durability	NPD (No Performance Declared)	

Table 3. Uses and advantages of Conplast SP 430 [9].

Uses

i. To provide excellent acceleration of strength gain at early ages and major increases in strength at all ages by significantly reducing water demand in a concrete mix.
ii. Particularly suitable for precast concrete and other high early strength requirements.
iii. To significantly improve the workability of site mixed and precast concrete without increasing water demand.
iv. To provide improved durability by increasing ultimate strengths and reducing concrete permeability.

Advantages

i. Major increases in strength at early ages without increased cement contents are of particular benefit in precast concrete, allowing earlier stripping times.
ii. Makes possible major reductions in water: cement ratio which allows the production of high-strength concrete without excessive cement contents.
iii. Use in the production of flowing concrete permits easier construction with quicker placing and compaction and reduced labour costs without increasing water content.
iv. Increased workability levels are maintained for longer than with ordinary sulphonated melamine admixtures.
v. Improved cohesion and particle dispersion minimises segregation and bleeding and improve pumpability.
vi. Chloride free, safe for use in prestressed and reinforced concrete

2. Materials and methods

2.1 Materials

The materials used are Ashaka Portland cement, rice husk ash, and Conplast SP 430 as the plasticizer. The cement conforms to BS EN 197 Part 1 [10] and was procured at the local market in Bauchi, Nigeria. The rice husk ash used to produce the ash was collected as a waste threshed out and separated from the rice grains. Therefore, it was collected as waste and calcined in the kiln of the industrial department of the university, at a temperature range of 400 °C to 600 °C, ground using a pestle and a mortar, and sieved using a sieve size of 150 µm. The physical and chemical properties were carried out in accordance with ASTM C 618-12 [11]. The cement chemical properties were tested at Ashaka Cement Company in Ashaka, Gombe State. The physical and chemical properties of the 'Ashaka' OPC and RHA are shown in **Table 4**.

Table 4. Physical and chemical properties of Ashaka Portland cement and rice husk ash.

Parameter	Cement	Rice husk ash
Physical properties		
Specific gravity	3.12	1.934
Fineness (%)	330 (kg/m^2)	20.2 (%)
Bulk density (kg/m^3) [ref]	830-1650	
Consistency (%)	29	
Initial setting time (min)	65	
Final setting time (min)	275	
Soundness (mm)	2.5	
LOI (%)	-	7.0
Chemical properties		
SiO_2	19.68	73.97
Al_2O_3	6.44	7.03
Fe_2O_3	3.32	1.19
CaO	60.92	0.96
MgO	0.97	2.45
SO_3	2.28	3.14
K_2O	0.85	2.78
Na_2O	0.12	0.90
TiO_2	0.30	Nil
P_2O_5	0.20	6.18
Mn_2O_3	0.20	1.40

2.2 Experiment

A mix proportion of 1:1.5:3, with a cement content of 370 kgm^{-3}, fine and coarse aggregates of 573 kgm^{-3}, and 1272 kgm^{-3}, respectively, and a water-cement ratio of 0.5. Using the Absolute Volume Method (ACI), it is a mix designed to have a minimum compressive strength of 25 Nmm^{-2} (M-25). Six (6) different mixes labeled MR-00, MR-10, MR-20, MR-30 MR-40, MR-50, and an improvement mix containing a 5.7 mL [12] dosage of Conplast SP 430 were used. They are designated as MR-00-CP to MR-50-CP and were cast. The concrete mix labeled MR-00/MR-00-CP is the control mix containing 0% of RHA/RHA-CP, while the other mixes labeled MR-10/MR-10-CP to MR-50/MR-CP-50, are RHA/RHA-CP, at 10%, 20%, 30%, 40%, and 50% replacement by wt. % of the ordinary Portland cement. A total of 180 concrete specimens (90 from each mix) were cast and cured for 3 to 90 days in a curing tank under laboratory conditions according to BS EN 12390 Part-2 [13]. Three samples were cast for each replacement level and tested for failure at the end of the curing regime. The above mix compositions were

used for the following experiments to determine the mechanical characteristics of the RHA-concrete. They are the slump, density, water absorption, and cube compressive strength.

The slump of RHA concrete

This property of the concrete was carried out in a fresh condition. The slump test determines how workable the concrete is. The standard slump cone for the slump test was used for the test by BS EN 12350: Part 2 [14] specifications on all batches of concrete produced. Three (3) tests were conducted for each batch, and the average of the results was taken. The results are shown in **Table 5**.

The density, water absorption, and cube compressive strength of RHA concrete

These tests were carried out in the hardened state of the concrete using cube molds of 100 mm. The density and water absorption were tested by BS EN 12390 Part 7 [15] and BS EN 1097-6 [16] respectively, while the compressive strength was tested in accordance with EN 12390-3 [17]. For the compressive strength a universal testing machine (Model CT-700) with a capacity of 100 tonnes, and a uniform rate of loading of 0.3 $kNmin^{-1}$ was used. **Table 6** shows the results of the slump, density, water absorption, and compressive strength of RHA concrete.

Table 5. Slump of RHA concrete.

Mix No	SP dosage (mL)	Slump (mm)
MR-00	-	15.88
MR-10	-	15.20
MR-20	-	11.50
MR-30	-	10.97
MR-40	-	10.34
MR-50	-	9.86
MR-00-CP	5.7	37.00
MR-10-CP	5.7	35.00
MR-20-CP	5.7	30.00
MR-30-CP	5.7	25.00
MR-40-CP	5.7	20.00
MR-50-CP	5.7	18.50

Table 6. Mechanical characteristics of RHA concrete.

Property	Mix No	SP dosage (mL)	Density (kgm^{-3})				
			3 days	7 days	28 days	60 days	90 days
Density (kgm^{-3})	MR-00	-	2610	2690	2660	2670	2550
	MR-10	-	2560	2610	2610	2630	2660
	MR-20	-	2580	2630	2570	2670	2620
	MR-30	-	2650	2490	2510	2580	2680
	MR-40	-	2320	2290	2360	2290	2240
	MR-50	-	2350	2310	2410	2460	2290
	MR-00-CP	5.7	2560	2620	2630	2650	2530
	MR-10-CP	5.7	2620	2680	2700	2610	2590
	MR-20-CP	5.7	2400	2420	2520	2540	2560
	MR-30-CP	5.7	2480	2570	2390	2520	2600
	MR-40-CP	5.7	2390	2370	2370	2500	2540
	MR-50-CP	5.7	2380	2360	2310	2340	2300

Table 6 continued

Property	Mix No	SP dosage (mL)	Density (kgm^{-3})				
			3 days	7 days	28 days	60 days	90 days
Water absorption (%)	MR-00	-	0.84	1.19	1.15	1.14	1.13
	MR-10	-	1.15	1.22	1.16	1.15	1.15
	MR-20	-	1.19	1.32	1.19	1.18	1.18
	MR-30	-	1.18	1.33	1.29	1.18	1.13
	MR-40	-	1.15	1.32	1.30	1.19	1.12
	MR-50	-	1.20	1.35	1.31	1.20	1.19
	MR-00-CP	5.7	0.77	0.86	0.77	0.77	0.76
	MR-10-CP	5.7	1.15	1.13	1.12	1.16	1.17
	MR-20-CP	5.7	1.18	1.28	1.19	1.21	1.19
	MR-30-CP	5.7	1.17	1.29	1.27	1.19	1.16
	MR-40-CP	5.7	1.18	1.19	1.20	1.12	1.06
	MR-50-CP	5.7	1.19	1.31	1.30	1.25	1.20
Compressive strength (Nmm^{-2})	MR-00	-	15.88	22.41	33.69	36.10	40.42
	MR-10	-	15.20	22.46	33.05	40.91	46.01
	MR-20	-	11.50	17.25	23.24	33.12	37.72
	MR-30	-	10.97	15.63	20.13	31.67	34.41
	MR-40	-	10.34	13.48	19.04	25.70	30.19
	MR-50	-	9.86	12.11	17.74	23.64	25.92
	MR-00-CP	5.7	15.58	22.35	33.59	39.60	43.67
	MR-10-CP	5.7	17.10	21.91	33.36	41.74	47.81
	MR-20-CP	5.7	12.99	16.68	30.51	37.53	40.52
	MR-30-CP	5.7	10.62	15.73	26.32	33.53	36.57
	MR-40-CP	5.7	10.35	13.45	20.31	28.33	32.92
	MR-50-CP	5.7	9.85	11.78	19.21	25.13	28.45

3. Statistical characteristics of RHA concrete

The data on the experiments using the cube compressive strengths were subjected to a sensitivity analysis test using the Minitab 18 Software. The purpose of this is to assess the integrity of the RHA concrete data collected. This was observed using two variables of measurements, the *Curing Age,* and the *Mix.* Data analysis is quantitative and refers to sets of processes by which numerical data are analyzed. Often, it involves the use of statistical modeling such as standard deviation, mean, etc., and the presentation of correlation tests between two or more variables of significance, ultimately arriving at a conclusion. **Table 7** refers to the situation when the concrete age was considered as the variable, and **Table 8** to the situation when the Mix is considered as the variable.

3.1 Correlation and P-value

Correlation factors are used to measure the strength of the linear relationship between two variables, and a correlation coefficient greater than zero indicates a positive relationship while a value less than zero signifies a negative relationship. The correlation coefficient is given as:

$$r = \frac{\sum (x_i - \overline{x})(y_i - \overline{y})}{\sqrt{\sum (x_i - \overline{x})^2 \sum (y_i - \overline{y})^2}} \quad [Correlation]$$

where r = correlation factor.

Tables 9 and 10 are cases for the two variables (age and mix) in consideration.

Table 7. Statistical characteristics of RHA/RHA-CP (curing).

Variable Age	Additions	Mean	SE mean	StDev	Variance	CoefVar	Range	95% CI	
								Lower	Upper
3 d	RHA only	12.29	1.06	2.59	6.69	21.04	6.02	10.40	14.18
7 d		17.22	1.80	4.41	19.40	25.58	10.35	14.01	20.44
28 d		24.48	2.91	7.12	50.75	29.10	15.95	19.28	29.69
60 d		31.86	2.63	6.43	41.40	20.20	17.27	27.16	36.56
90 d		35.78	2.95	7.22	52.06	20.17	20.09	30.51	41.05
3 d	RHA + 5.7 mL Conplast	12.75	1.23	3.02	9.14	23.71	7.25	10.54	14.96
7 d		16.98	1.77	4.34	18.86	25.57	10.57	13.81	20.16
28 d		27.22	2.59	6.35	40.36	23.34	14.38	22.58	31.86
60 d		34.31	2.67	6.55	42.84	19.08	16.61	29.53	39.09
90 d		38.32	2.90	7.12	50.63	18.57	19.36	33.13	45.52

Table 8. Statistical characteristics of RHA/RHA-CP (mix).

Variable Mix	Additions	Mean	SE mean	StDev	Variance	CoefVar	Range	95% CI	
								Lower	Upper
M-0	RHA	29.70	4.56	10.20	103.98	34.33	24.54	21.71	37.69
M-10		31.53	5.70	12.74	162.22	40.40	30.81	21.54	41.51
M-20		24.57	4.86	10.87	118.05	44.23	26.22	16.05	33.08
M-30		22.56	4.54	10.14	102.92	44.96	23.44	14.61	30.52
M-40		19.75	3.69	8.26	68.19	41.81	19.85	13.28	26.22
M-50		17.85	3.13	6.99	48.86	39.15	16.06	10.37	23.33
M-0-CP	RHA + 5.7 mL Conplast	30.96	5.26	11.77	138.45	38.01	28.09	21.73	40.18
M-10-CP		32.38	5.79	12.94	167.44	39.96	30.71	22.24	42.53
M-20-CP		27.65	5.51	12.32	151.67	44.55	27.53	17.99	37.30
M-30-CP		24.55	5.00	11.18	125.02	45.54	25.95	15.79	33.32
M-40-CP		21.07	4.28	9.57	91.67	45.44	22.57	13.57	28.58
M-50-CP		18.88	3.62	8.10	65.68	42.92	18.60	12.53	25.24

3.2 Covariance

Covariance and correlation are very helpful in understanding the relationship between two continuous variables. Covariance tells whether both variables vary in the same direction (positive covariance) or in the opposite direction (negative covariance). Covariance between two variables x and y can be calculated as follows:

Tables 11 and 12 are results of the two variables, age and mix.

Table 9. Correlation and P-values of RHA concrete (curing).

Age	Addition	3 d	7 d	28 d	60 d
7 d	RHA only	0.98 (0.001)			
28 d		1.00 (0.000)	0.98 (0.000)		
60 d		0.88 (0.022)	0.95 (0.004)	0.89 (0.016)	
90 d		0.87 (0.023)	0.95 (0.003)	0.90 (0.015)	0.99 (0.000)
7 d	RHA + 5.7 mL Conplast	0.96 (0.003)			
28 d		0.91 (0.012)	0.95 (0.004)		
60 d		0.92 (0.010)	0.94 (0.005)	0.99 (0.000)	
90 d		0.95 (0.004)	0.95 (0.003)	0.96 (0.002)	0.99 (0.000)

Table 10. Correlation and P-value of RHA concrete (mix).

Mix	Additions	M-0	M-10	M-20	M-30	M-40
M-10	RHA only	0.99 (0.002)				
M-20		0.96(0.010)	0.99 (0.001)			
M-30		0.93 (0.020)	0.98 (0.004)	1.00 (0.000)		
M-40		0.96 (0.010)	0.99 (0.001)	1.00 (0.000)	0.99 (0.001)	
M-50		0.97 (0.008)	0.99 (0.001)	1.00 (0.000)	0.99 (0.001)	1.00 (0.000)
M-10	RHA + 5.7 mL Conplast	0.99 (0.002)				
M-20		0.96 (0.010)	0.99 (0.001)			
M-30		0.93 (0.020)	0.98 (0.004)	1.00 (0.000)		
M-40		0.96 (0.010)	0.99 (0.001)	1.00 (0.000)	0.99 (0.001)	
M-50		0.97 (0.008)	0.99 (0.001)	1.00 (0.000)	0.99 (0.001)	1.00 (0.000)

Table 11. Covariance of RHA concrete (curing).

Age	Additions	3 d	7 d	28 d	60 d	90 d
3 d	RHA only	6.69				
7 d		11.13	19.40			
28 d		18.34	30.87459	50.75		
60 d		14.56	26.96203	40.96	41.40	
90 d		16.31	30.24291	46.17	46.09	52.06
3 d	RHA + 5.7 mL Conplast	9.14				
7 d		12.56	18.86			
28 d		17.45	26.13	40.36		
60 d		18.14	26.78	41.09	42.84	
90 d		20.45	29.49	43.51	46.03	50.63

Table 12. Covariance of RHA concrete (mix).

Mix	Additions	M-0	M-10	M-20	M-30	M-40	M-50
M-0	RHA only	103.98					
M-10		128.28	162.22				
M-20		106.09	137.10	118.05			
M-30		96.58	126.37	109.79	102.92		
M-40		80.73	104.11	89.50	83.04	68.19	
M-50		68.85	88.38	75.55	70.23	57.49	48.86
M-0-CP	RHA + 5.7 mL Conplast	138.45					
M-10-CP		151.18	167.44				
M-20-CP		144.10	158.18	151.67			
M-30-CP		131.30	144.11	137.36	125.02		
M-40-CP		110.46	123.41	115.70	105.71	91.67	
M-50-CP		94.13	104.70	99.03	90.04	77.36	65.68

4. Discussion

4.1 Workability of RHA concrete

The workability of concrete is the ease of placing concrete. This property of concrete is affected by some factors like water content, mix proportion, aggregate size, shape, grading, texture, and the use of admixture. The slumps of the rice hush ash concrete and that to which 5.7 mL Conplast SP 430 are shown in **Figure 1**. The performance of CP is evaluated in three (3) stages: a) control mix; b) addition of RHA, and c) addition of CP to RHA, respectively.

The purpose of the addition of CP to a concrete mix is to limit the water demand while improving workability. Thus, the addition of CP to concrete achieved a consistency of 37 mm, compared to the control mix. This is lower than the manufacturer's specification of ≥ 120 mm. This is approximately 69% lower than the specified. Additions of RHA to the mix achieved a consistency range of 15.2 mm to 9.9 mm, a reduction in workability of 4.3% to 37.9%. This behavior has been attributed to the texture and amorphous nature of the RHA [5]. The addition of CP to concrete-RHA mix recorded a consistency range of 30 mm to 18.5 mm. Superplasticizers (SPs) are generally negatively charged (anionic) polymers, which tend to adsorb the positively charged (cationic) surfaces and the products formed from the hydration process. RHA particles are porous, and the CP polymers may get trapped in the pores. This is presumed to hinder dispersion by steric repulsion, compromising the efficiency to enhance the workability [6]. This could be seen as a reduction of 18.9% to 50.0%, respectively.

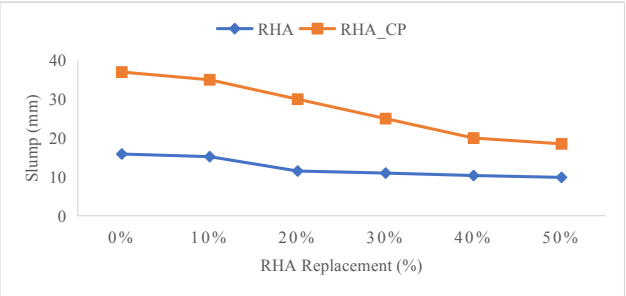

Figure 1. Slump of RHA/RHA-CP concrete.

4.2 Water absorption of RHA concrete

The water absorption of RHA concrete is a function of the characteristics of the constituent materials of the concrete. The levels to which the addition of CP admixture has transformed the concrete mix (Control) are evaluated from the results given in **Table 5**. This shows the addition of CP to concrete has a decreasing effect on water absorption. This ranges from 8.3% to 33% as the age of concrete increases. Therefore, it can be concluded that the addition of CP reduces the water absorption and densifies the concrete. This is in line with the assertions of the

manufacturers (≥ 12%) [9]. On average 26.8% can be assumed to be achieved when CP is used in concrete.

The effect of adding RHA to a concrete mix from the experimental data shows the reverse. The water absorption increased rather than decrease. The same findings have been acknowledged by previous research and have been attributed to the texture and amorphous nature of RHA [5]. Not only that RHA is a porous material that has a very large specific surface area, but also has an angular structure [7,8], as shown in **Figure 2**. However, this increase reduces as curing progresses, but increases as the percentage replacement of cement by wt. % of RHA continues. It is equally noticed with interest the high-water absorption recorded for the early age of 3 days. This occurs from 10% to 50% replacements. To be able to have a realistic evaluation of how RHA did affect the water absorption, the total average is calculated, and this is 12.8%. Therefore, the addition of RHA to concrete will increase the water absorption by approximately 12.8%.

The effect of adding CP to RHA concrete mixture was also evaluated. The results from **Table 6** show that this addition did not reduce the water absorption but rather increased the water absorption. This behavior may be a compatibility problem between the admixture CP-SP430 and the RHA. A total average of 52.9% is recorded as an increase. These total averages of 12.8% and 52.9% respectively, for RHA and RHA-CP, are based on comparing the performances of RHA and RHA-CP, with their control mixes respectively. The results are remarkable. Therefore, further investigations on the compatibility of RHA and CP are advocated. Evaluating the effect of CP on the mixes, RHA and RHA-CP minimal reduction of approximately 1.4% on the replacement levels is observed. This can be a further pointer to the fact that the use of CP as an admixture with RHA may not be compatible.

4.3 Density of RHA/RHA-CP concrete

The density of a material is an important property that is tied to the characteristics like the strength of the material. The evaluation of the density of RHA and RHA-CP shows that additions of RHA and RHA-CP to a concrete mix are beneficial up to 30%, for RHA and RHA-CP, respectively, giving rise to densities ≥ 2400 kgm^{-3} ((Nor/Concrete). These satisfy their appropriateness to be used for reinforced concrete. Replacements from 40% to 50% could be used appropriately for lightweight concrete since their densities are ≥ 2200 ≤ 2400 kgm^{-3} (L/Concrete). However, it is seen from **Table 13** that there are abnormalities at 60 days and 90 days at 40% replacement, which registered densities ≥ 2400 kgm^{-3}. One of the reasons for the high values of the densities registered is because of the pozzolanic actions of the RHA and the impact of the CP admixture.

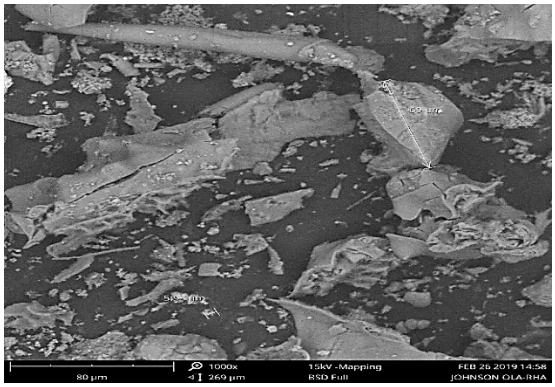

Figure 2. Scanning electron microscope (SEM) image of a RHA particle.

4.4 Compressive strength of RHA/RHA-CP concrete

Figures 3a and 3b are plots of the compressive strengths of RHA, and RHA-CP concrete obtained from **Table 6**. The characteristics depicted by the two mixes are similar. Both have their maximum compressive strengths at a maximum replacement of 10%. The addition of CP therefore seems not have visible effects on the maximum replacement level. It is also observed that the effectiveness of the addition of CP admixture starts after 28 days of curing. This is confirmed by the reductions recorded from 3 days to 28 days (1.9%, 0.3%, 0.3%).

Table 14 shows the classification chart useful as a tool for concrete works specifications. Three (3) classes of concrete grades are identified, and these

are as follows:

a. Blinding concrete whose strength is < 15 kNm^{-2}. (blinding)

b. Lintel concrete > 15 $kNmm^{-2}$ < 20 kNm^{-2}. (lintel)

c. Reinforced concrete > 20 kNm^{-2}. (r/concrete)

4.5 Statistical characteristics

The mean represents the average value in a dataset and is important because it gives us an idea of where the centre value is in a dataset. It is also important because it carries a piece of information from *every* observation in a dataset. **Figures 4a and 4b** show the distribution of the means for RHA and RHA-CP mix, respectively. The effects show generally that both the RHA and the addition of Conplast to RHA gave a gradual increase in the mean as the age of the concrete increased. While, for **Figure 4a** the increase is pronounced from 28 days of curing and continues until 90 days however, minimally. For **Figure 4b**, the maximum mean is at 10% both for RHA and RHA-CP. Thus, it could be inferred that

Table 13. Density classification of RHA/RHA-CP.

Type	*Repl (%)*	*3 d*	*7 d*	*28 d*	*60 d*	*90 d*
RHA	10	Nor/Concrete	Nor/Concrete	Nor/Concrete	Nor/Concrete	Nor/Concrete
	20	Nor/Concrete	Nor/Concrete	Nor/Concrete	Nor/Concrete	Nor/Concrete
	30	Nor/Concrete	Nor/Concrete	Nor/Concrete	Nor/Concrete	Nor/Concrete
	40	LW/Concrete	LW/Concrete	LW/Concrete	LW/Concrete	LW/Concrete
	50	LW/Concrete	LW/Concrete	LW/Concrete	LW/Concrete	LW/Concrete
RHA-CP	10	Nor/Concrete	Nor/Concrete	Nor/Concrete	Nor/Concrete	Nor/Concrete
	20	Nor/Concrete	Nor/Concrete	Nor/Concrete	Nor/Concrete	Nor/Concrete
	30	Nor/Concrete	Nor/Concrete	Nor/Concrete	Nor/Concrete	Nor/Concrete
	40	LW/Concrete	LW/Concrete	LW/Concrete	LW/Concrete	LW/Concrete
	50	LW/Concrete	LW/Concrete	LW/Concrete	LW/Concrete	LW/Concrete

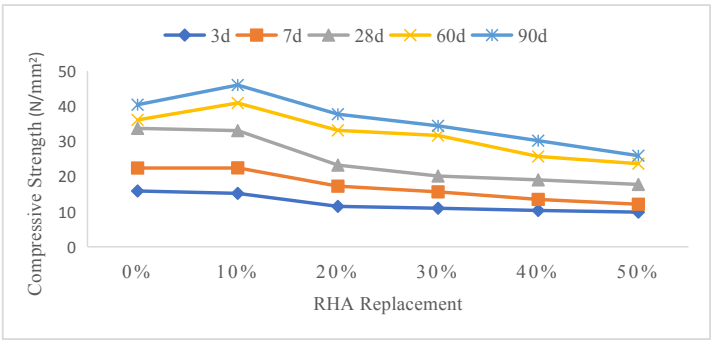

(a)

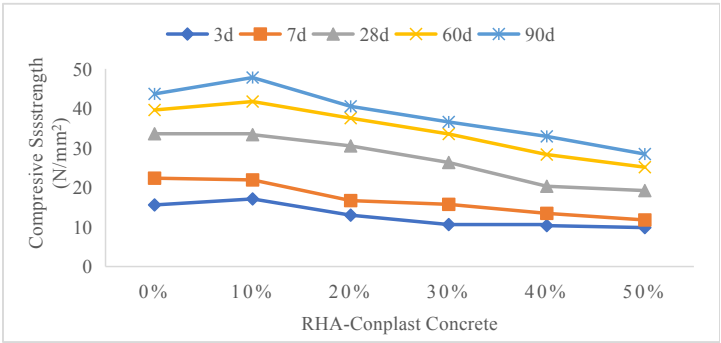

(b)

Figure 3. Compressive strength of RHA/RHA-CP concrete.

both RHA and the use of Conplast are beneficial to the concrete mixture.

The characteristics of the data in **Table 7** have specifics. It shows that the values of the coefficient of variation (COV) are 21.04, 25.58, 29.10, and 20.20. These data reflect the size of the standard deviation to the mean and show consistency of performance. The consistent performance is further confirmed by the confidence limit (CI), which shows that the mean falls within the limits of CI.

Table 15 further shows the characteristics of the RHA/RHA-CP concrete based on the correlation and covariance analysis and their implications. As highlighted previously **Correlation** tells us both the strength and the direction of this relationship, while **Covariance** indicates the extent to which two random variables increase or decrease in tandem with each other. These principles of analysis are applied to the two variables of consideration the Curing and the Mix, respectively. The results of the analysis shown in **Table 15** confirm the acceptability of using CP with RHA. The correlation and correlation factors are high. Equally the covariances along the row (Age, days) and down the column (Replacement %) exhibit notable characteristics, confirming the maximum performance at 10% replacement [5].

Table 14. Strength classification chart of RHA/RHA-CP.

Type	*Repl (%)*	*3 d*	*7 d*	*28 d*	*60 d*	*90 d*
	10	blinding	r/concrete	r/concrete	r/concrete	r/concrete
	20	lintel	blinding	r/concrete	r/concrete	r/concrete
RHA	30	lintel	blinding	r/concrete	r/concrete	r/concrete
	40	lintel	lintel	blinding	r/concrete	r/concrete
	50	lintel	lintel	blinding	r/concrete	r/concrete
	10	blinding	r/concrete	r/concrete	r/concrete	r/concrete
	20	lintel	blinding	r/concrete	r/concrete	r/concrete
RHA_CP	30	lintel	blinding	r/concrete	r/concrete	r/concrete
	40	lintel	lintel	r/concrete	r/concrete	r/concrete
	50	lintel	lintel	r/concrete	r/concrete	r/concrete

Table 15. Correlation and P-value, covariance of RHA/RHA-CP.

Variable	**Type**	**Correlation**		**Covariance**	
		r^2	(ρ)	Row	Column
Curing	RHA	$0.88 \leq r < 1.0$	$0.023 \leq \rho \leq 0.005$	Increase	Decrease
	RHA-CP	$0.91 \leq r < 1.00$	$0.012 \leq \rho < 0.005$	Increase	Increase
Mix	RHA	$0.93 \leq r < 1.0$	$0.020 \leq \rho < 0.005$	Max-10% > 10% Decrease	Max-10% > 10% Decrease
	RHA-CP	$0.93 \leq r < 1.0$	$0.020 \leq \rho < 0.005$	Max-10% > 10% Decrease	Max-10% > 10% Decrease

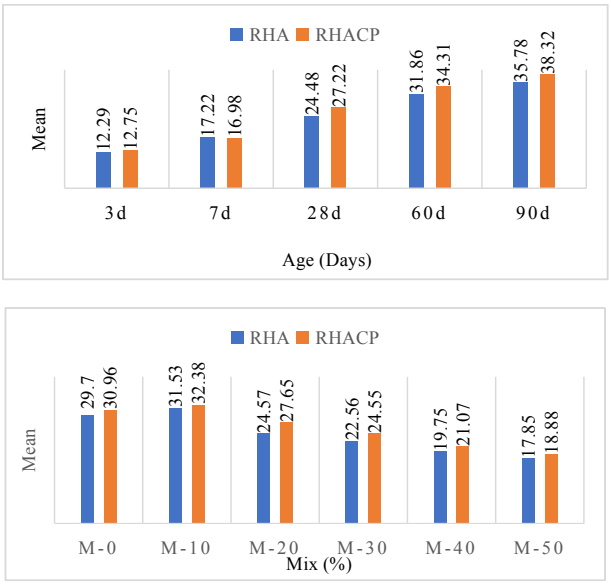

Figure 4. Mean values of RHA/RHA-CP.

5. Conclusions

This work presents an evaluation test on CP admixture and its effects on concrete and concrete-RHA mixes. The conclusions are as follows:

The addition of CP admixture to concrete (Control) improved the workability marginally and reduced water absorption. While the addition of RHA to concrete reduced the workability because of its texture which absorbs water and increased the water absorption. The texture of RHA and the non-compatibility of CP with RHA are probable factors that caused the water absorption to increase when RHA and CP are used together.

The densities and the compressive strengths of RHA and RHA-CP concrete are high and good for reinforced concrete. The maximum strength of 25 kNm^{-3} is achieved at 10% replacement.

The statistical characteristics of the results on the test samples of the concrete-RHA and concrete-RHA-CP mixes show that the use of RHA and CP admixture for concrete production produces reliable concrete. The means of the test results and other characteristics are within the derived limits. The correlations (r^2) and correlation factors (ρ) show good interactions between the concrete parameters. The covariances confirm that hydration proceeded as curing continues confirming the maximum replacement to be at 10%.

Conflict of Interest

There is no conflict of interest.

References

[1] Arrigoni, A., Panesar, D.K., Duhamel, M., et al., 2020. Life cycle greenhouse gas emissions of concrete containing supplementary cementitious materials: Cut-off vs. substitution. Journal of Cleaner Production. 263, 121465.

[2] Rehan, R., Nehdi, M., 2005. Carbon dioxide emissions and climate change: Policy implications for the cement industry. Environmental Science & Policy. 8(2), 105-114.

[3] Rahla, K.M., Mateus, R., Bragança, L., 2019. Comparative sustainability assessment of binary blended concretes using Supplementary Cementitious Materials (SCMs) and Ordinary Portland Cement (OPC). Journal of Cleaner Production. 220, 445-459.

[4] Supino, S., Malandrino, O., Testa, M., et al., 2016. Sustainability in the EU cement industry: The Italian and German experiences. Journal of Cleaner Production. 112, 430-442.

[5] Uchechukwu, E.A., Olakunle, J.O., Duna, S., 2022. Characteristics of ordinary Portland cement paste containing rice husk ash and conplast. Journal of Building Material Science. 4(1), 1-10.

[6] Van Tuan, N., Ye, G., Van Breugel, K., et al., 2011. The study of using rice husk ash to produce ultra high performance concrete. Construction and Building Materials. 25(4), 2030-2035.

[7] Cordeiro, G.C., Toledo Filho, R.D., Tavares, L.M., et al., 2011. Influence of particle size and specific surface area on the pozzolanic activity of residual rice husk ash. Cement and Concrete Composites. 33(5), 529-534.

[8] Chao-Lung, H., Le Anh-Tuan, B., Chun-Tsun, C., 2011. Effect of rice husk ash on the strength and durability characteristics of concrete. Con-

struction and Building Materials. 25(9), 3768-3772.

[9] ASTM C 494-92: Standard Specification for Chemical Admixtures for Concrete [Internet]. Available from: https://www.astm.org/c0494_c0494m-19e01.html

[10] Fosroc Conplast SP430 [Internet]. Available from: https://fosroc.com/assets/HotSpotDocuments/Conplast-SP430.pdf

[11] BS EN 197-1:2011. Cement Part 1: Composition, Specifications, and Conformity Criteria for Common Cements [Internet]. Available from: https://knowledge.bsigroup.com/products/cement-composition-specifications-and-conformity-criteria-for-common-cements/standard

[12] ASTM C 618-12: Standard Specification for Coal Fly Ash and Raw or Calcined Natural Pozzolan for Use in Concrete [Internet]. Available from: https://webstore.ansi.org/standards/astm/astmc61812

[13] BS EN 12390-2:2019. Testing Hardened Concrete-Making and Curing Specimens for Strength Tests [Internet]. Available from: https://knowledge.bsigroup.com/products/testing-hardened-concrete-making-and-curing-specimens-for-strength-tests-2/tracked-changes

[14] Elinwa, A., 2018. Mechanical strength of admixed Conplast SP 430 cement paste and concrete. Available from: https://ssrn.com/abstract=3174640 or http://dx.doi.org/10.2139/ssrn.3174640

[15] BS EN 12350-2:2019. Testing Fresh Concrete-Slump Test [Internet]. Available from: https://knowledge.bsigroup.com/products/testing-fresh-concrete-slump-test-2/tracked-changes

[16] BS EN 12390-7:2009. Testing Hardened Concrete Part 7: Density of Hardened Concrete [Internet]. Available from: https://standards.iteh.ai/catalog/standards/cen/5c244c2e-9414-4a0d-97db-96b3a2ddcc9b/en-12390-7-2009

[17] EN 1097-6:2022. Testing for Mechanical and Physical Properties of Aggregates-Part 6: Determination of Particle Density and Water Absorption [Internet]. Available from: https://standards.iteh.ai/catalog/standards/cen/7eb55eec-cf2d-449c-bdf5-45534b169181/en-1097-6-2022

[18] BS EN 12390-3:2019. Testing Hardened Concrete Part 3: Compressive Strength of Test Specimens [Internet]. Available from: https://standards.iteh.ai/catalog/standards/cen/7eb738ef-44af-436c-ab8e-e6561571302c/en-12390-3-2019

BILINGUAL PUBLISHING GROUP

Journal of Building Material Science

https://journals.bilpubgroup.com/index.php/jbms

ARTICLE

Matrix-Material Fabrication Technique and Thermogravimetric Analysis of Banana Fiber Reinforced Polypropylene Composites

***Nazrul Islam*[1*], *M. A Gafur*[2]**

[1] *Department of Basic Sciences, Primeasia University, Dhaka, 1213, Bangladesh*

[2] *Pilot Plant and Process Development Centre (PP & PDC), Bangladesh Council of Scientific and Industrial Research (BCSIR), Dhaka, 1205, Bangladesh*

ABSTRACT

From the environmental consideration, it would be very interesting to use natural fibers such as banana, jute or coir as reinforcement materials instead of artificial fibers or any kind of synthetic materials. Natural fibers have many advantages over synthetic ones. Polypropylene banana fiber composites (PPBC) are prepared using untreated and alkali-treated banana fibers at 10-25% by weight of the fiber loading. The thermal properties of polypropylene natural fiber composites are very important for technological uses. Thermogravimetric measurements show that the incorporation of banana fiber into PP enhances the thermal stability of composites containing treated fibers, in comparison with untreated fibers. A composite of biodegradable polypropylene (PP) reinforced with short banana natural fibers was prepared by melt blending followed by a hot press molding system. The thermal properties of matrix materials were studied using thermogravimetric analyzers TGA units. It is observed that the introduction of short banana fibers slightly improved the thermo oxidative stability of PP-banana composites. Physical and chemical changes occurred through dehydration, phase transition, molecular orientation, crystallinity disruption, oxidation and decomposition, and incorporation of several functional groups. Systematic investigations of the thermal behavior of polymers in gas, vacuum or inert atmosphere give the knowledge of how change takes place in polymers. To understand such changes thermogravimetric analysis (TGA) and thermal analysis (TG) were performed. It is observed reinforcement of short banana fiber leads to little improvement in the thermooxidative stability of PPBC. Due to the enhancement of thermo-mechanical properties, such composites may be used as building materials namely roof materials, selling materials and many other engineering applications.

Keywords: Polypropylene banana composites (PPBC); Natural fiber; Oxidative stability; Thermogravimetric analysis (TGA); Decomposition

*CORRESPONDING AUTHOR:

Nazrul Islam, Department of Basic Sciences, Primeasia University, Dhaka, 1213, Bangladesh; Email: n_islam58@yahoo.com

ARTICLE INFO

Received: 4 May 2023 | Revised: 7 October 2023 | Accepted: 10 October 2023 | Published Online: 6 November 2023

DOI: https://doi.org/10.30564/jbms.v5i2.5700

CITATION

Islam, N., Gafur, M.A., 2023. Matrix-Material Fabrication Technique and Thermogravimetric Analysis of Banana Fiber Reinforced Polypropylene Composites. Journal of Building Material Science. 5(2): 15-24. DOI: https://doi.org/10.30564/jbms.v5i2.5700

COPYRIGHT

Copyright © 2023 by the author(s). Published by Bilingual Publishing Group. This is an open access article under the Creative Commons Attribution-NonCommercial 4.0 International (CC BY-NC 4.0) License. (https://creativecommons.org/licenses/by-nc/4.0/).

1. Introduction

There are many popular reinforcing fibers that are commonly used in the preparation of composites. In technological consideration, natural fiber composites are considered to be the most promising candidate. The term thermal analysis refers to experimental techniques used to study temperature dependent properties of materials [1-4]. Reinforcement of the natural fibers organic and inorganic polymers causes changes in their structural, physical, mechanical, and chemical properties. To study such changes in thermal properties thermogravimetric analysis (TGA) is conveniently used. To understand the behavior of treated and untreated PPBC, the mechanical properties are very significant ingredients to study. We have also studied tensile and flexural strength with different fiber loading % of PPBC. The results of the physical and mechanical properties of PPBC have already been studied by Islam et al. [5]. DTA techniques typically enable us to detect the thermal reactions and effects associated with chemical or physical changes in materials as they pass through a transition due to heating or cooling [6]. There are many methods have been proposed and employed for the estimation of kinetic parameters from dynamic thermogravimetric analysis (TGA) [7].

In the present article, we reported banana-polypropylene composites prepared by using a very typical process developed by us. The thermal properties of polypropylene composites reinforced with untreated and alkali-treated banana fibers, PPBC are also studied in the present article. Very little scientific literature is available on the thermal stability of banana composites. Thermal analysis of untreated and chemically treated banana fibers was studied by Rana et al. [8] and the jute composite was studied by Mitra et al. [9]. The main influencing factors on the properties of composites are matrix structure, treatment or processing, and the use of fillers or reinforcements [10]. Furthermore, TG was performed for analysis and comparison purposes. The successful blending of PP and natural fibers has provided an easy way to improve the thermal properties of PPBC and create a fully biodegradable material.

The analytical experimental technique to investigate the temperature dependent behavior of a sample is popularly known to be thermal analysis [2]. There are so many polymers available today and they decomposed over distinct temperature ranges leaving behind certain proportions of volatiles and residues. TGA is a very efficient analytical technique to measure the weight loss of a test sample over a temperature range. TGA provides significant information about the stability and decomposition of polymer materials by studying volatile and residues. Significantly, the TGA trace can also be used to study the moisture content, volatile and plasticizer, and ashes, which of course extend for cross-linked polymers.

The thermal energy is supplied to the polymer in thermal analysis which results evolve of moisture content at low temperatures (80 °C to 110°C). The polymer species starts losing beyond this temperature range. The decomposition temperature is the range at which the polymer starts degrading and maintaining the process up to complete decomposition. The TGA curve traces relatively a simple sigmoidal path for many polymers. The TG curve mostly changed by the kinetic parameters: i) reaction order, n; ii) rate constant, k; iii) frequency factor, A; and iv) activation energy, Ea. The elucidation mechanism of polymer degradation and thermal stability has a great impact on the values of these parameters. The TG curves may be complex if a polymer degrades by a multi-step mechanism. A number of methods have been proposed and employed for the estimation of kinetic parameters from dynamic thermogravimetric analysis (TGA) studies [6,7]. TGA offers a viable alternative to furnace aging. The materials are heated at various distinct rates including their decomposition region of temperature. Then the decomposition temperature is determined from the thermal curve.

2. Experimental

2.1 Materials

The sample polypropylene (PP T101) used in the present observation has a specific gravity of 0.9. Banana fibers were collected from PP and PDC, BC-

SIR, Dhaka and Bangladesh. To remove the moisture the chopped fiber was annealed at 110 °C for 24 hours. The approximate dimensions of the chopped fiber were 2-3 mm in length and 2 mm in width (DIN IS03310/1, w = 2 mm, FRITSCH). The moisture from PP granules was removed following the same procedure of annealing. Characteristics of the raw materials (banana fiber) are presented below. We have used the commercially available PP; therefore one may consider supplied values for different properties by the manufacturer.

Characteristics of raw materials

Banana fiber:

Physical properties:

Ultimate:

1) Length in mm	: 80-280
2) Diameter/width in mm	: 0.011-0.034
3) Cell width (m)	

Single fiber:

1) Density (apparent) gm/cc	: 0.86-0.62
2) True density gm/cc	: 1.33-1.31
3) Moisture regain at 65% RH	: 10-12
4) Porosity	: 35-53

Mechanical properties:

1) Tensile strength in KP	: 3.53
2) Fiber twist in TPC	: 5.75
3) Elongation %	: 37

Chemical composition of banana fiber:

1) Cellulose	: 65.112%
2) Hemicellulose	: 17.325%
3) Pectin & related compound	: 2.124%
4) Legnin	: 8.018%
5) Ash, wax	: 2.502%
6) Others	: 4.919%

Electrical properties:

1) Volume resistivity : 6.5-7 $\times 10^5$ cm at 65% RH

2) Dielectric strength for 0.1 m length of fiber: 5.0 KV

2.2 Alkali treatment

To perform alkali treatment 20% NaOH was taken in a RB flask. Then the required amount of fibers was poured into this solution and kept for 15 minutes at ambient temperature. The fibers were then moved to another container for cleaning and washing with distilled water. It was then neutralized by using a solution of low concentration sulfuric acid. The samples were washed again with distilled water following the method prescribed by Guha Roy et al. [10] and then air dried for 48 hours in an oven.

2.3 Composite fabrication

We have prepared a polymeric matrix by compression modeling using Paul-Otto-Weber hydraulic press as shown in **Figure 1**, which is explained in reference [2]. We have used a type die of inner diameter of 146 mm and an outer diameter is 158 mm having two discs of 7.5 on each side. During molding we have to maintain a temperature of 250 °C and 40 kN pressure. As the mold is closed under applied pressure the materials are squeezed between the two halves and brought into two desired shapes within the mold. Some materials flow out of the mold in the form of thin film which is known to be "flash". The compacted mass becomes cured and hardened to shape due to heating. After cooling the mold is given a desired shape as requirement.

Thermal and other properties of the plastic and textile materials are to be molded, widely controlled by the actual temperature and pressure. Heat and pressure are introduced in a single stroke in polymer materials and fiber for compression modeling. This is achieved on a heated plate by hydraulic press. For drying, controlled and treated PP and banana fibers (chopped) were kept in an oven at 110 °C for the duration of one hour. For mixing fiber and PP were blended for two minutes with 400 rpm at room temperature. Then small quantity of releasing agent was added to the mixture and put into a die or mold. In Paul Otto Weber press machine 50 kN initial load was applied from the top of the mold having a dimension of (6 × 6 square inches). The temperature in the electrical heater was then set to 80 °C. It only took 25-30 minutes to reach a temperature of 180 °C. It took only 25-30 minutes to reach this temperature and the system was kept at 180 °C for 20 minutes. To achieve the required thickness and also to avoid any void a final load of up to 100 kN was applied from

the top of the sample. Then the heating system was stopped and the specimen was cooled by flowing water over the outer area of the heating plate. After cooling the specimen was separated from the mold. Following ASTM procedure D-2307 compact pellet of circular shape was prepared using cork-borer at high pressure.

Figure 1. Weber Pressen hydraulic press.

2.4 Thermogravimetric analysis (TGA)

TGA traces of untreated and treated PP fiber composite samples were recorded using a thermal analyzer controlled by a computer interfaced controller. TG/DTA 6300 system along with an EXSTAR 6000 controller (Seiko Instruments Inc., Japan) which uses a horizontal system balancing mechanism to collect data. The profile of the thermal stability of the sample composite was observed at temperature 30-600 °C with 20 °C·min^{-1} heating rate.

2.5 Measurement of thermal properties

Nitrogen environment was maintained to perform TGA experiment. Samples of ≤ 30 mg were calcineted up to 600 charred at a heating rate of 20 °C·min^{-1} while nitrogen was inserted at a rate of 100 mL/min. The programmed controlled converter is used to keep the temperature of the furnace at the required state. As a reference material, we used alumina. In TGA a measuring range was set to ≤ 30 mg and, 1500 μV. During the process for first 25% of the weight loss sample was considered for the rest of the calculations subsequently.

3. Result and discussion

3.1 Thermal behavior

Figure 1(a) shows the TG curves for PP, banana fiber, and PP-B composites respectively in a static nitrogen environment at a heating rate of 20 °C·min^{-1}. While **Figure 1(b)** shows the TG curves for both treated and untreated banana fibers. In **Figure 1(a)** top line is for PP, the bottom one is for banana fiber and mid line represents the composite respectively. It is revealed from the figure TG curve for composite lies between banana fiber and PP. The weight loss of the composites is due to the loss of moisture loss as it contains only 10% fiber. The major degradation occurs in a single step for fiber and PP although there is a small degradation observed for fiber at low temperature due to moisture loss, while it occurs in two steps for composite. In the case of composite the cause of initial loss is due to fiber and the second step is due to the degradation of PP. The $T_{5\%}$ and T_{max} represent the temperature at which 5% and maximum weight loss occur respectively are presented in **Table 1** for both untreated and treated fibers and composites. **Figure 1(a)** reveals that, for both treated and untreated fibers *T5%* and *Tmax* increase steadily with the increase of PP content. Its underlying cause is that PP has a higher $T_{5\%}$ and T_{max} than that of the fibers. **Table 2** shows that the TGA data in the first step weight losses under nitrogen environment for untreated and treated fiber, take place at 250.12-300.76 °C with 13.87% weight loss and at 280.35-311.06 °C with a 12.92% weight loss respectively. On the other hand the first step wt. losses occur at 320.01-360.36 °C with 15.63% wt. loss and at 322.14-372.74 °C with 16.04% wt. loss for untreated and treated fiber-PP composites respectively. The second

stage or major wt. loss starts at 360.12-472.45 °C with 82.402% wt. loss and at 372.14-488.02 °C with 77.20% wt. loss for untreated and treated fiber-composites respectively. The weight percentages remaining at 500 °C are 0.65% and 1.30% for untreated and treated fibers and 2.01% and 3.21% for untreated and treated PP-B composites respectively. This must be the decomposition of PP. The T_{max} values of the PP-B composites seem to be higher than those of the PP-B composites in the untreated state. Therefore, introducing treated fibers into the pp matrix leads to improvement of the composite having alkali-treated fibers are higher than those containing fiber of untreated states. Strong NaOH has been successfully used for removing lignin, hemicelluloses, and other alkali-soluble compounds from the surface of the fiber. This increases the number of reactive hydroxyl groups on the surface of the fiber and remains available for chemical bonding [2].

Figures 2(a) and 2(b) represent the DTG curves for the PP and PP-B composites for untreated and treated fibers respectively. The major weight loss peak occurs at 365.15-488.45 °C for the PP-B composite. The weight loss in the first region are mostly occurred due to the moisture or loosely bound untreated elements which may not closely related to any change in structure. We may interpret the second region as the loss of non-constitutional or hydrogen evolution, low molecular hydrocarbon and may also be due to few oxygen-containing compounds. The wide peak of DTG curve carries the significance of the maximum weight loss at T_{max} [2]. In all the cases, there is slightly more char formation in the non-compatibilized composite. The underlying cause of weight loss in this region occurred due to oxidative thermal breakdown of the composite materials and expulsion of higher molecular mass hydrocarbons and CO_2, CO etc. like oxygen containing compounds.

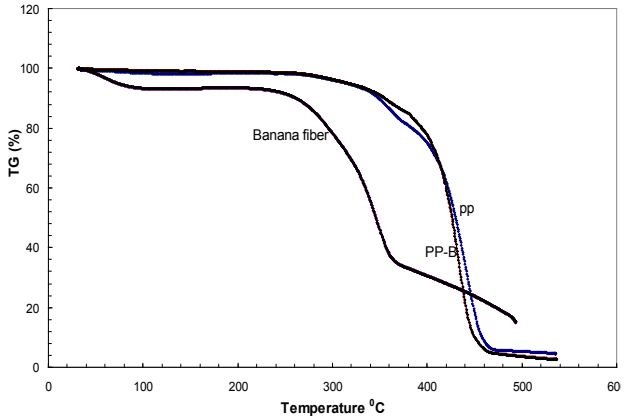

Figure 1(a). TG profile of PP, banana fiber and PPBC.

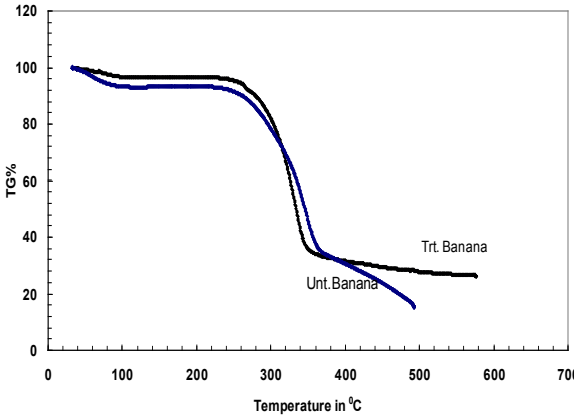

Figure 1(b). TG profile of treated and untreated banana fiber of PPBC.

Table 1. Thermal properties of banana fiber, PP and PP-B composites.

Specimen	T^1_{max} (°C)	T^2_{max} (°C)	$T_{5\%}$ (°C)
Untreated fiber	300.76	391.00	109.90
Treated fiber	311.06	420.50	253.91
PP-B (untreated)	360.96	472.45	318.04
PP	370.63	478.45	320.50
PP-B (treated)	372.14	488.02	338.9

Table 2. Weight loss of PP, untreated and Alkali treated banana fiber composites.

Weight % specimen	First stage		Second stage		Remaining at 500 °C
	Temperature (°C)	Weight loss (%)	Temperature (°C)	Weight loss (%)	
Untreated fiber	250.12-300.76	13.87	300.76-391.00	80.32	0.65
Treated fiber	280.35-311.06	12.92	311.06-420.50	81.26	1.30
PP	300.00-370.63	14.52	370.63-478.45	84.46	0.1
PP-B(untreated)	320.11-360.96	15.63	360.12-472.45	80.40	2.01
PP-B (treated)	322.14-372.14	16.04	372.10-488.00	77.21	3.21

It is thus seen that the oxidative thermal breakdown in the backbone chains of the PP composite occurs at higher temperatures. The DTG peak for PP-B composites and PP at around 450 °C may be due to the oxidative reaction, of corresponding TGA trace. The DTG thermo gram of treated PP-B composite in **Figures 2(a) and 2(b)** also show one small.

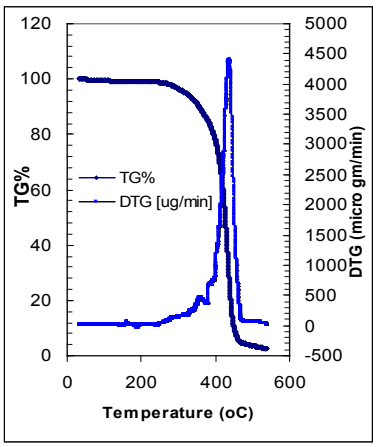

Figure 2(a). TG% and DTG profile for untreated treated PPBC.

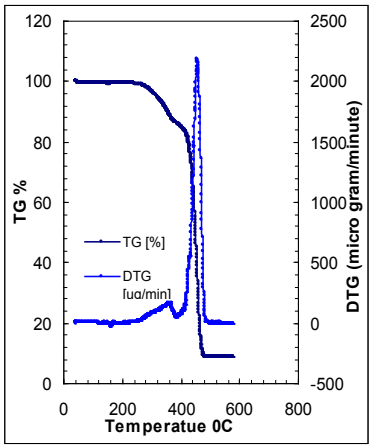

Figure 2(b). TG% and DTG profile for PPBC.

Transition/phase changes at (380 ± 5) °C, and one big transition/phase changes with an exothermic peak at (460 ± 5) °C. Thus, it is seen that the thermal stability of the composite remains stable up to the temperature of 500 °C. We have shown similar thermal behavior in our previous reports [11-13].

To obtain the kinetic parameters from the TG traces of fibers and PP-B composites differential method is used following the arguments of Sharp-Wentworth [2] considering the order of reaction 1/2 and 1. **Figures 3(a)-3(d)** also represent the differential method for n = 1/2 and n = 1 as $\frac{1}{T^2} log2\left[1-(1-\alpha)^{\frac{1}{2}}\right]$ against $\frac{1}{T}$ for both untreated and treated banana fiber and PP-B composites respectively. For n = 1/2 this method is found less satisfactory, because the experimental points do not fit straight lines that well in all the different regions (A, B, C) of the curves rather than deviate to form a curved path in accordance with equation $\frac{d\alpha/\mathrm{dT}}{(1-\alpha)^n} = \frac{A}{\beta} exp\left(\frac{-E_0}{RT}\right)$.

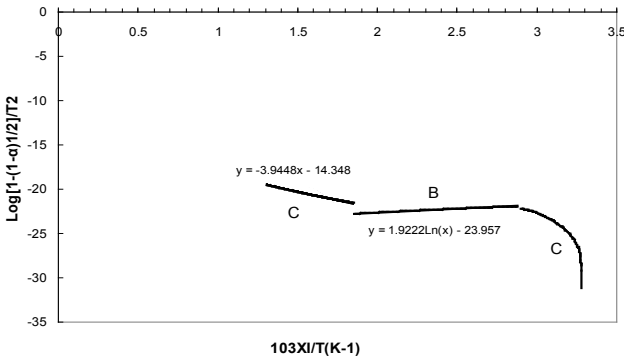

Figure 3(a). log2[1–(1–α)$^{1/2}$]/T^2 against 10^3 × 1/T graph for untreated banana fiber.

It is seen that for n = 1, the experimental points of TG traces for both fibers and composites have been

found to fit straight lines in all the different regions (A, B, C). Thus, the reaction order of composites may be considered as 1. The activation energies in different regions for all the methods were calculated and depicted for both the fibers and composites in **Table 3**.

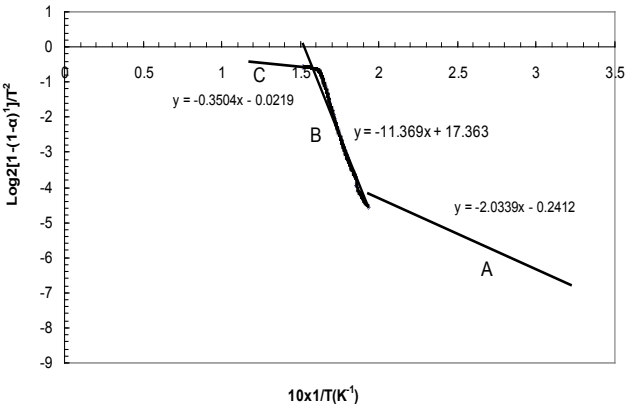

Figure 3(b). $\log2[1–(1–\alpha)^{1/2}]/T^2$ against $10^3 \times 1/T$ graph for treated banana fiber.

The activation energies for reaction in all the transformation modes are smaller for alkali-treated fiber and PP-fiber composites while it is compared to the untreated fiber and PP-fiber composites. This means that the alkali-treated PP-fiber composites emit more thermal energy at high-temperature regions. Thus, it can be inferred from the above discussion that PP-fiber composite stabilizes on alkali–treatment. This fact can be well understood from the relative increase in the intensity of the IR transmission band and thereby the structure stabilization of PP-fiber composites [14].

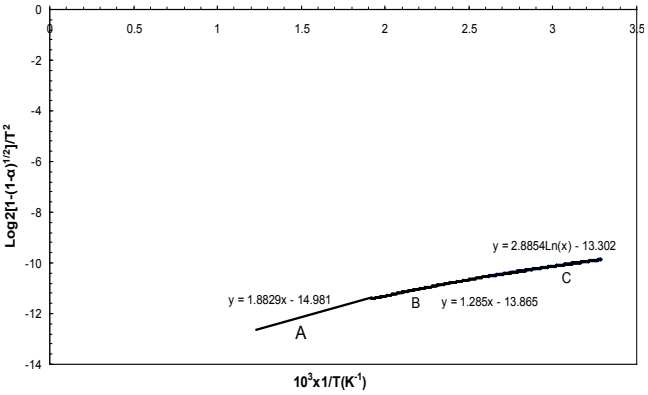

Figure 3(c). $\log2[1–(1–\alpha)^{1/2}]/T^2$ against $10^3 \times 1/T$ graph for untreated banana fiber.

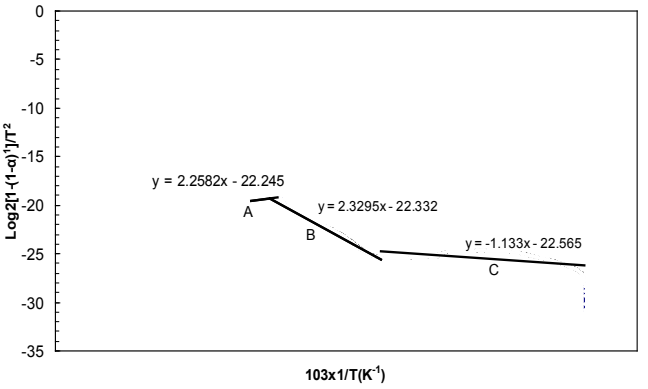

Figure 3(d). $\log2[1–(1–\alpha)^{1/2}]/T^2$ against $10^3 \times 1/T$ graph for untreated banana fiber.

Table 3. Temperature range, mass loss %, activation energies of fiber and PP-B composites.

Description of the materials	Temperature (K)	Mass loss %	Activation energy, En (KJ/mole)		Remarks
			DM n = 1/2	DM n = 1	
Untreated banana fiber	305.25-523.12 Step C	5.16 ± 1	0.9278	0.282	H_2O and non constitutional elements evolved.
	523.12-573.76 Step B	13.87 ± 1	0.036	0.0468	Low molecular mass hydro-carbons evolved. Expulsion of high.
	573.76-664.49 Step A	80.32 ± 1	0.0754	0.107	molecular mass hydro-carbons and CO, CO_2 etc
Treated banana fiber	312.30-553.35 Step C	4.52 ± 1	0.0177	0.0389	H_2O and non constitutional elements evolved.
	553.35-584.06 Step B	12.92 ± 1	0.2047	0.2175	Low molecular mass hydrocarbons evolved
	548.06-693.50 Step A	81.26 ± 1	0.0316	0.7049	Expulsion of high molecular mass hydrocarbon CO, CO_2 etc.

Table 3 continued

Description of the materials	Temperature (K)	Mass loss %	Activation energy, En (KJ/mole)		Remarks
			DM n = 1/2	DM n = 1	
Untreated PP-B composite	303.22-593.11 Step C	2.21 ± 1	0.0532	0.0389	H_2O and non constitutional elements evolved.
	593.11-633.96 Step B	15.63	0.2459	0.0114	Low molecular mass hydrocarbons evolved.
	633.96-745.45 Step A	80.40 ± 1	0.0554	0.0163	Expulsion of high molecular mass hydrocarbons and CO, CO_2 etc.
Treated PP-B composite	595.14-645.14 step C	3.42 ± 1	0.0196	0.0216	H_2O and non constitutional elements evolved.
	645.14-761.02 step B	15.63 ± 1	0.1922	0.1786	Low molecular mass hydrocarbons evolved.
	310.69-595.14 Step A	77.21 ± 1	0.0435	0.0446	Expulsion of high molecular mass hydrocarbons and CO, CO_2 etc.

4. Conclusions

- Short banana fibers reinforced in PP composites were prepared by a melt mixing process which is followed by the hot press compression molding. The role of NaOH in PPBCs is very significant in improving the adhesion of banana fiber with polypropylene matrix [15,16].
- It is observed from the thermo gravimetric measurements that the addition of banana fibers into PP causes an increase in the decomposition and the thermal stability of composites in the case of treated fibers then seems to improve while it is compared to the untreated fiber. It is also seen that the value of $T_{5\%}$ and T_{max} are higher for the composites containing treated fibers, than the composites containing untreated fiber. This phenomenon carries the information that the PPB is more hydrophilic than PP.
- We may conclude from the greater overall thermal stability of PPB treated composites over untreated PPBC. We can see from the reference [14] that the FTIR report suggests no structural changes due to the presence of lignin in the alkali treated banana fibers. Therefore the addition of such treated fibers into the pp matrix leads to the improvement of the thermal stability of the composites. So we may also conclude that the composites remain thermally stable up to the temperature 500 °C.
- Weight loss takes place due to oxidative thermal breakdown of the composite structure and expulsion of higher molecular mass hydrocarbons, and the compounds containing oxygen like CO_2, CO, etc. The oxidative thermal breakdown in the backbone chains of the PP composite is therefore found to occur at higher temperatures. Moreover the initial low tempts. weight loss occurs due to the removal of the solvent polymer matrix. The major weight loss occurs at higher tempt. Due to degradation and volatization of PP along with fiber present in the composite.
- In TGA curve the weight loss of the composites is due to the loss of moisture loss as it contains only 10% fiber. The major degradation occurs in a single step for fiber and PP although there is a small degradation observed for fiber at low temperature due to moisture loss, while it occurs in two-step for composite. In the case of composite the cause of initial loss is due to fiber and the second step is due to the degradation of PP.
- The DTG peak near the temperature 500 °C may be due to the oxidative reaction, of the corresponding TGA curve. The weight percentages remaining at 500 °C are 0.65% and 1.25% for untreated and treated fibers and 0.06% and 1.25% for untreated and treated PP-B composites respectively. This must be the decomposition of PP. The T_{max} values of the PP-B composites seem to be higher than those of the PP-B composites in the untreated state. Therefore, introducing treated fibers into the pp matrix leads to improvement of the composite having

alkali-treated fibers are higher than those containing fiber of untreated states.

- The activation energies for reaction in all the transformation modes are greater than is being obtained for alkali-treated fiber and PP-fiber composites when they are compared with the untreated fiber and PP-fiber composites. The alkali-treated PP-fiber composites emit more thermal energy and stabilize at high-temperature regions.
- PPBC also poses better thermal stability and excellent moisture properties. The environmentally friendly behavior of PPBC makes it very popular in various engineering applications like the automotive and construction industry. Decomposition and thermal stability rates are lower in untreated PPBC in comparison with treated PPBC.

Author Contributions

Most of the experiential works are performed under the guidance of M. A. Gafur in BSIR Lab. Experiments and analysis of the data manuscript are carried out and prepared by Md. Nazrul Islam.

Conflict of Interest

There is neither a conflict of interest nor any financial obligation from any funding agency work.

Acknowledgment

The authors acknowledge BCSIR Dhaka, Bangladesh for extending support by providing their fabrication and thermal analysis facilities in the pilot plant laboratory.

References

[1] Keattch, C.J., Dollimore, D., 1969. An introduction to thermogravimetry. Heyden & Son Ltd.: New York.

[2] Hatakeyama, T., Quinn, F.X., 1999. Thermal analysis: Fundamentals and applications to polymer science. John Wiley & Sons Ltd.: London.

[3] Katsikas, L., Jeremic, K., Jovanovic, S., et al., 1993. The thermal degradation kinetics of dextran and pullulan. Journal of Thermal Analysis and Calorimetry. 40(2), 511-517.

[4] Eroğlu, M.S., Akilli, M.M., Güven, O., 1997. Spectroscopic, thermal, and mechanical characterization of carboxyl-terminated polybutadiene-based carbon black-filled networks. Journal of Applied Polymer Science. 66(2), 355-366.

[5] Islam, Md. Nazrul, Gafur, M. A. and Khan, Amir Hussain, 2007. Natural fiber-polypropylene (Banana-PP) matrix composites- fabrication and study of mechanical properties: Jahangirnagar Physics Studies, 13, 1-7.

[6] Rajulu, A.V., Rao, G.B., Rao, B.R.P., et al., 2002. Properties of ligno-cellulose fiber *Hildegardia*. Journal of Applied Polymer Science. 84(12), 2216-2221.

[7] Pal, S.K., Mukhopadhyay, D., Sanyal, S.K., et al., 1988. Studies on process variables for natural fiber composites—effect of polyesteramide polyol as interfacial agent. Journal of Applied Polymer Science. 35(4), 973-985.

[8] Rana, A.K., Basak, R.K., Mitra, B.C., et al., 1997. Studies of acetylation of jute using simplified procedure and its characterization. Journal of Applied Polymer Science. 64(8), 1517-1523.

[9] Mitra, B.C., Basak, R.K., Sarkar, M., 1998. Studies on jute-reinforced composites, its limitations, and some solutions through chemical modifications of fibers. Journal of Applied Polymer Science. 67(6), 1093-1100.

[10] Guha Roy, T.K., Chatterjee, S., Adhikari, D., et al., 1988. Studies on the bleaching of jute. Journal of the Textile Institute. 79(1), 108-125.

[11] Liaw, D.J., Lee, W.F., 1985. Thermal degradation of poly [3-dimethyl (methylmethacryloylethyl) ammonium propanesulfonate]. Journal of Applied Polymer Science. 30(12), 4697-4706.

[12] Lee, W.F., 1989. Comparative study of various methods for thermal degradation of poly [3-dimethyl (methacryloyloxyethyl) ammonium propanesulfonate]. Journal of Applied Polymer Science. 37(11), 3263-3275.

[13] Lee, W.F., Tsai, C.C., 1994. Aqueous solution properties of poly (trimethyl acrylamido propyl

ammonium iodide) [poly (TMAAI)]. Journal of Applied Polymer Science. 52(10), 1447-1458.

[14] Niehuis, E., Heller, T., Feld, H., et al., 1987. Design and performance of a reflectron based time-of-flight secondary ion mass spectrometer with electrodynamic primary ion mass separation. Journal of Vacuum Science & Technology A: Vacuum, Surfaces, and Films. 5(4), 1243-1246.

[15] Chand, N., Vashishtha, S.R., 2000. Development, structure and strength properties of PP/PMMA/FA blends. Bulletin of Materials Science. 23, 103-107.

[16] Ray, D., Sarkar, B.K., Rana, A.K., et al., 2001. The mechanical properties of vinylester resin matrix composites reinforced with alkali-treated jute fibres. Composites Part A: Applied Science and Manufacturing. 32(1), 119-127.

BILINGUAL PUBLISHING GROUP

Journal of Building Material Science

https://journals.bilpubgroup.com/index.php/jbms

REVIEW

Application of Nanotechnology in Soil Stabilization

***Amit Kumar*[1*], *Kiran Devi*[2]**

[1] *Civil Engineering Department, NIT Kurukshetra, Kurukshetra, 136119, India*

[2] *Civil Engineering Department, SGT University, Gurugram, 122505, India*

ABSTRACT

Nano-technology is expanding its horizon in various science and technology fields. In civil engineering, soil is a complex material and used for various functions and applications. Meanwhile, sometimes an effective soil stabilization technique is needed to fulfil the site criteria and can be achieved by adopting various methods e.g., physical, chemical, thermal or reinforcement using geotextiles and fabrics. The mechanism of soil stabilization using nanomaterials is still unexplored and open to prospective researchers. The present article attempts to touch and explore the possibilities of nano-technology in soil improvement and its applications in various civil engineering works. Microstructural analysis of the nanomaterials treated soils using the latest equipment has also been discussed. The study interprets that the use of nano materials is still limited, due to their high cost and sophisticated handling procedures. Though the use of nanoparticles in soil stabilization results in extraordinary improvements in various soil properties, the improved soil properties could be utilized for various geotechnical projects. The present study bridges the past findings to the present scenario of nanomaterials in soil improvement.

Keywords: Nano particles; Fine soils; Geotechnical engineering; Microstructural analysis; Field application

1. Introduction

Natural soil is very complex and essential for all living organisms on the Earth. Every species of the plants including shrubs, cactus, mushrooms etc. has their unique functions in maintaining the ecosystem [1,2]. Naturally, the plants stabilized the soil beneath the civil structures but unfortunately, humans have not appreciated and cited the fact to date [3-5]. Plants also help to check natural disasters like floods and liquefaction conditions surrounding the erected structures. The fact is that the roots of the plants

*CORRESPONDING AUTHOR:
Amit Kumar, Civil Engineering Department, NIT Kurukshetra, Kurukshetra, 136119, India; Email: kauleamit0089@gmail.com

ARTICLE INFO
Received: 19 August 2023 | Revised: 10 November 2023 | Accepted: 20 November 2023 | Published Online: 22 November 2023
DOI: https://doi.org/10.30564/jbms.v5i2.5913

CITATION
Kumar, A., Devi, K., 2023. Application of Nanotechnology in Soil Stabilization. Journal of Building Material Science. 5(2): 25-36. DOI: https://doi.org/10.30564/jbms.v5i2.5913

COPYRIGHT
Copyright © 2023 by the author(s). Published by Bilingual Publishing Group. This is an open access article under the Creative Commons Attribution-NonCommercial 4.0 International (CC BY-NC 4.0) License. (https://creativecommons.org/licenses/by-nc/4.0/).

serve as fibers in the soil matrix. A lot of studies conclude that foresting is necessary to prevent air as well as noise pollution [3,6].

Soil stabilization generally modifies and upgrades the soil properties required at the site. This can be done by various methods or sometimes a combination of methods is required [7,8]. The admixtures used and mixed in the soils alter the inherent soil properties and improve the engineering behavior of the soils. Likewise, sand mixing is done to reduce the liquefaction action in the soils [9,10]. Basically, the addition of external materials to the soils is done through two methods; in the first case, natural soils mixed with other stabilizing materials get improved mechanically after changing their gradation and in the later case, the materials react and fill the voids after penetration like jet grouting [11].

Modern nanotechnology is ruling in various fields including engineering. Nanomaterials, by definition, are nanometre sized particles and are considered as a whole unit. In soil mechanics, the clay size varies from 1-2 μm and is a nanoparticle itself. The application of nanomaterials in geotechnical engineering could ingress the new large size particles of concern [12]. But, still some issues as listed follow can hurdle the game changing nano materials: a. Dearth knowledge of basic physics and chemistry to understand the behavior of nanoparticles; b. Unskilled labour; c. Dearer price of the nano materials.

Although there are certain obstacles that deter the widespread adoption of nanomaterials for soil enhancement, researchers have undertaken significant investigations into the use of nanomaterials in soil stabilization. This article provides an overview of the topic, covering the classification, properties, methodologies, advantages, and disadvantages of nanomaterials in the context of soil improvement. Additionally, the article offers suggestions for future directions in this field.

2. Classifications of nanomaterials

A nanoparticle is incredibly small, measuring in the range of 1 to 100 nanometers in size. There is a significant difference between the mechanism applied for soil stabilization to conventional strengthening materials. This difference could be pronounced by the fact that these materials have a larger area to volume ratio irrespective of the shape of the particle and their quantum effects derived from spatial confinement [13]. Nanomaterials can be classified as zero dimensional (0D) or also known as quasi-zero dimensional i.e., having aspect ratio from 1-∞; one dimensional (1D) those have one dimension outside the nanoscale, two dimensional (2D) in which two dimensions are not of nanoscale, three dimensional (3D) also known as bulk nanomaterials and all the dimensions of this kind of nanostructures lie above 100 nm [14]. **Table 1** contains the typical examples of all category nanomaterials.

Table 1. Typical examples of classified nanomaterials.

Type of nanostructure	Examples
0D	Nanograins, Nanoshells, Nanocapsules, Nanorings, Fullerenes, Colloidal Particles, Nanoporous silicon, Quasi-crystals
1D	Nanorods, Nanofilaments, Nanotubes, Quantum wires, Nanowires, Imogolite, Halloysite, Palygorskite, Sepiolite
2D	Discs, Paltelets, Ultrathin films, Superlattices, Quantum wells, Kaolinite, Illite, Smectite, Chlorite, Vermiculite
3D	Bundled nanowires and nanotubes

Though each type of nanomaterial serves specific purposes, 1D nanostructured materials are particularly crucial for applications related to energy, sensing, and biomedical fields. Therefore, it is prudent to explore 1D nanomaterials extensively to gain deeper insights into research involving nanomaterials.

3. Properties of nanostructures

It is a fact that the nanomaterials are of microscopic size therefore, their various physical, chemical and structural properties could serve many functions at the point of their applications. The magnetic, electrical and optical properties of the nanomaterials have wide applications in different fields.

3.1 Structural properties

Structural properties of a material are those

properties that express information about the role of the elements in the overall structure of the system. Nanoparticles have a regular crystalline structure and follow a kind of magical number [15]. Scientists believe that the unusual behavior of the nanomaterials is due to their exceptionally high surface area to volume ratio [16,17]. Structural properties of the nanoparticles can only be observed by sophisticated laboratory instruments e.g., X-ray Diffraction (XRD), Scanning Electron Microscopy (SEM), Small-Angle X-ray Scattering (SAXS), Transmission Electron Microscopy (TEM), Scanning Probe Microscopy (SPM) and Gas Adsorption. The size of the particles can get altered under different laboratory conditions e.g., time, mixing method and additive type etc. [18-20].

In the case of soil stabilization, gelling (gel formation due to chemical reactions) due to nanosilica totally depends upon the mean particle size of nanosilica. As a general guideline, the smaller the particle size will be, the faster the gelling and bonding will be [21]. Nanoparticles produce the bond between soil and admixture, which has some cohesion until the bond gets torn apart along the shear plane [22].

3.2 Physical and chemical properties

In general, the physical properties of material comprise of color, texture, appearance, melting point, fire point etc. whereas common chemical properties are media concentration, reaction with fluids etc. In exceptional, some interesting properties of different nanomaterials can be scribed as gold nanoparticles show the different absorbing capacity to red color with respect to its size i.e., the larger size (90 nm) absorbs the red and the smaller size (30 nm) reflects the red color. Nanostructured TiO_2 has self-cleansing properties but it loses this when used in bulk. Nano gypsum is much harder (3x) than other conventional micro-sized particles [23-27]. Unique chemical properties of the nanomaterials could be used for storing energy from bulk to nano materials, increasing germination in the plants etc. [28,29].

3.3 Mixing methods

Agglomeration during mixing is a common problem associated with the nanomaterials. Hence, when employing nanomaterials for soil stabilization, it is advisable to utilize mixing techniques that reduce agglomeration to ensure effective results. Homogeneous mixing is the key factor in getting the expected results. Researchers have adopted various mixing methods to get a uniform soil-additive mix and added dispersing agents drop by drop to evade the agglomeration effects during mixing. Another important precaution to consider is periodically agitating the mixture to maintain its effectiveness during the soil stabilization process. Additionally, the fusion of two nanomaterials is necessary while dealing with two or more nano sized additives simultaneously [30]. Most of the researchers recommend a water sprinkling on the mix right after mixing the nanomaterials into the soil. A thorough mixing and agitation of the mix is also recommended to get a homogeneous mix [31-36].

3.4 Interaction mechanism

Though understanding the fundamental mechanisms and microstructural behavior of the stabilized soil is not that easy but latest techniques and insights gained through various research made some rational and valid theories to explain the same [37,38]. In the 70's, Lambe and Whitman summarized that the behavior of soil at the macro level is controlled by the interaction at the micro level. During this, the mineralogical and chemical compositions of the stabilized soils are dependent upon the structural rearrangement and environment in which the reactions take place [39,40]. The theories developed in the past say that the cohesion in the soil is the result of attraction forces developed in the soil particles. The swelling characteristics of the soil can be judged after observing the presence of a smectite group in the soil, which is highly vulnerable to swelling and shrinkage. Haematite and geothite (iron oxides) vary in sizes from 10-100 nm and soil containing these oxides can produce a hardened product [41]. High thermal conductivity, an indirect method for predicting dry density and gradation, is more in sands containing silica with respect to the sands containing mica. High clay content imparts the swelling characteristics to the

soils, which is also a function of high plasticity. Surface forces in clays are higher than sands and silts. On a thumb rule, high clay content in the soils is responsible for high plasticity and high swell-shrinkage properties in fine-grained soils. Hence, having a profound understanding of soil composition at the micro level can significantly simplify the comprehension of anticipated soil behavior [40,41].

3.5 Microstructural imaging

Microstructural characterization of the specimens is a very efficient and effective tool to analyze the changes that occurred after the soil stabilization using nanomaterials. The microstructural patterns and images are used to study the bonding, cracks, chemical and physical changes in the soils. Though there are numerous microstructural analysis techniques e.g., SEM, XRD, TEM, Field Emission Scanning Electron Microscopy (FESEM), Fourier Transform Infrared Spectroscopy (FTIR), Thermogravimetric Analysis (TGA) and X-ray Fluorescence Spectroscopy (XRF) and so on, but a prior knowledge on these techniques is highly recommended. Micro images are the easiest way to interpret the structural and mineralogical changes in the soils [42]. Among all techniques, SEM is believed to be excellent and can be coupled with the EDX or XRD/XRF. TEM has a different sampling procedure but is an authentic microscopy technique. This technique not only measures the size and shape of the particle but also supplies other relevant information. Atomic Force Microscopy (AFM) has a unique feature that can be used in the presence of air, water and vacuum. XRD is also a simple and cheap technique to know the mineralogy of the nanomaterials [42,43]. On the basis of previous studies, it can also be interpreted that there is no validation method other than microstructural analysis to check the dispersion of nanomaterials and penetration of cementitious gel (gelling) in the soil [43].

4. Soil-nanomaterial interactions

The scarcity of usable land has levied a challenge to the geotechnical engineers to repair the weak soil deposits so that construction can be executed at those sites too. So, the engineers are making efforts to improve the engineering performance of the soils by adding wastes, fibers and nanoparticles. The following subsections summarize the changes that occurred in various soil properties after adding the nanoparticles into different soils.

4.1 Plastic properties

In comparison to alumina, copper nanoparticles were found more effective in decreasing the plasticity index of the soil [44]. Nanoclay has contradictory effects on the plasticity index of fine soils. Some researchers claim that nanoclay decreased the plasticity index up to a satisfactory level while others are in favor of an increase in plasticity index. The quantity of nanoclay to be added to the soil varies from 1%-8%, according to the nature of the soil [45-49]. The reason behind this could be the expansive nature of nanoclay [45]. Whereas, the addition of clayey nano soil, alumina, copper, CuO, MgO, TiO_2, nano flyash, nanopolymer of polypropylene, MgO, zeolite, nanolime, carbon nanotubes and nanofibers, all decreased the plasticity index due to their high densities and lesser surface area than clay and silica [37,44,45,49-53]. The liquid limit of soil directly correlates to the compressibility of that soil. The high compressibility of any soil corresponds to a high liquid limit. The increase in liquid limit could be due to the water absorption capacity of added nanoparticles. Such variations in the results may occur due to the dissimilarities in the soil origin, deposit and type. Therefore, during conducting the experiments, any experimental error, factor and correction must be taken care of.

4.2 Compaction properties

Research conducted using copper and alumina nanoparticles showed that high density copper nanoparticles increased the maximum dry density but, high dosage of nanoparticles started to agglomerate, which caused an increase in void ratio and a decrease in the dry density of soil. Copper nanoparticles agglomer-

ate less than alumina, because copper nanoparticles are about 2 times bigger in size than alumina [45]. TiO_2, nano flyash, nanoclay and nanoparticles also have the same effects on compaction properties [48,51]. An increase in maximum dry density could be an effect of rearranging and cementation between soil particles. Nanoclay showed the reverse effect on silty clay i.e., a decrease in maximum dry density and increase in optimum moisture content have been reported. A probable reason for decreased dry density was flocculation and agglomeration of soil particles and cation exchange reaction. But sometimes, lesser specific gravity and pozzolanic reactions could also be the reasons for the reverse effects [37,52,54,55].

4.3 Strength properties

Nanomaterials improved the strength characteristics of various types of soils up to a satisfactory level. Nano-Z solution increased the CBR strength of soil by forming the siloxane bonds. These bonds are similar to natural primary valence bonds found in the soils. Nano sized additives fill the voids faster and behave like a sealant in the soils. This hydrophobicity in the soils is created by long alkyl chains. These chains help to adsorb the water from soil voids and consequently decrease the plasticity of the soil. Thus, an ion change mechanism in the soil ultimately produces hydrophobic material [50]. 3% of nanosilica has improved the CBR of the lime stabilized clay. The amount of nanosilica in the range of 0.7% is found as optimum because beyond this, the benefits of nanosilica become limited [56,57]. Nanoclay is also found excellent stabilizer for fine grained soils when used at 1.5% by weight of dry soil [58,59]. It also increases the shear strength and decreases the angle of refraction when mixed in the silty soil [55,60]. But, freeze and thaw cycles decrease the compressive strength [61]. Nano particles have a positive effect on the thixotropy of the soil. Thixotropy is the property of the soil by which soil regains strength without any moisture change and is very important to be known by geotechnical engineers [48]. Nanosilica in the range of 0.7% adversely affects the strength properties of the soil and this amount can be considered as optimum. The micro imaging of the soil samples also confirmed the absorption of water in the matrix [57]. The improvement in the strength of the cement treated soil could occur due to an increase in the hydration process. Pozzolanic effects, crystallization and filling effects can also be other reasons for the strength gain in the soils [62]. Calcium silicate hydrous (CSH) gel formation with calcium hydroxide $Ca(OH)_2$ was also observed through scanning images. However the formation of $Ca(OH)_2$ is not good for strength properties of the soils. Nanoparticles in the cement treated soil infuse like an atom and generate the prevailing linkage between particles. This infusion becomes easy due to a larger specific surface area and higher specific energy. Moreover, beyond the optimum amount, the reactions reverse and generate a high amount of calcium hydroxide which weakens the bonding and imparts the cracks in the soil specimens. Colloidal silica grouting arrests the liquefaction in the soils. Various researchers suggest to use 5%-20% colloidal silica [10,63,64]. In the case of sand, void fillers relocate the sand particles and prolong the development of pore pressure in the media [65]. Nanoclay contains a larger specific area than nanosilica and consequently can be considered as much better for collapsible soils. Interlocking effects and chemical reactions are also other effects of nanoclay.

4.4 Hydraulic conductivity

The hydraulic conductivity of soil is very close to permeability and therefore, is an important property of the soil when the soil is to be used for lining purposes or when applied as an impermeable layer. Experiments conducted on sand grouted with colloidal silica show that the grouting material reduces the hydraulic conductivity. On a graph, this decrease followed an exponential curve. Such property of a nanostructure could be beneficial for barrier systems [65]. Bentonite soil specimens of low concentration have proved more resistive than high concentration bentonite specimens. This proves that low bentonite content can be used where no effect of bentonite is to be considered [45]. Nano CuO and γ-Al_2O_3 particles clogged the voids in clayey soil specimens and hence

reduced the hydraulic conductivity of the specimens. Nano cloisite showed an inverse relationship with hydraulic conductivity [35,61]. Nano structured multiwall tubes and carbon nanofibers both also were found excellent in decreasing hydraulic conductivity. Surprisingly, nanoiron particles did not show any noticeable variation in the hydraulic conductivity of the fine soils [66]. This all happened due to the blocking phenomenon which restrains the flow to maintain uniformity while another phenomenon ripening is related to a decrease in porosity and permeability [53]. Bentonite, nanoclay, nanoalumina also has no significant effect on hydraulic conductivity but decrease the desiccation cracks in the soil. This property of the materials can be used during the lining of canals [44]. Nanosilica of sizes i.e., 15 nm and 80 nm, decreased the hydraulic conductivity and, 15 nm nanosilica was found more effective than 80 nm due to their higher particle density [67]. Nano particles of more than 0.8% increased the hydraulic conductivity due to the adsorption of more water. Moreover, nanoparticles in excess quantity, agglomerate and leave the voids behind consequently triggering the water movement through the media and increasing the permeability.

4.5 Consolidation and shrinkage

Consolidation is a natural process, in which soil voids change gradually under pressure over time. This property of fine-grained soils has its own pros and cons. Sometimes, consolidation is good for compaction purposes while on the other hand consolidation could be disastrous when the foundation of the superstructure gets settled. In the row, iron oxides and allophone clays reduced the consolidation settlement [68]. Nano particles of TiO_2 and flyash reduced the consolidation characteristics of soft soil. Both additives reduced the consolidation settlement by 60% and 67% respectively [51]. Nanoclay, NanoMgO, Nanoalumina were also found very effective in reducing the consolidation settlement by about half and increasing the load carrying capacity by almost by 50%-60% [48,69,70]. Generally, consolidation settlement is less under loading conditions, when nanoparticles are added to the soil. Because water gets replaced by the nanoparticles and increases the density of the treated soil. Moreover, the remaining water could be utilized during ion exchange which is instant after adding the additives. Research proves that 0.7%, 0.3% and 0.2% are the optimum amounts of NanoCuO, NanoMgO and Nanoclay to improve the strength properties of organic soils. Polypropylene homopolymer eliminates the swelling behavior of clayey soils. This is due to hydrophobic nature imparted by the fibers in the soils. Nanoclay also has the same effects on fine-grained soils [37,62]. Nanoparticles are not cost-effective so, their use in commercial applications is still questionable. Further research to explore the toxicity spreading in the field is also a concern [71].

4.6 Field applications

A limited number of studies have been conducted on the field testing and applications of nanoparticles' treated soils. The primary reason for the limited utilization of nanomaterials at construction sites is a lack of fundamental knowledge in mixing, testing, and assessing their performance. However, sand stabilized with Nanosilica is in use. This all is made possible by the fact that in nanosilica treated sands, the reactions can be controlled at the field by adjusting the pH and salt concentrations of the silica solution. Colloidal silica has a unique property to alter its viscosity by adjusting pH and ionic content. Although, limited pressure application restricts its use in sands [72]. Reduction in hydraulic conductivity is a benefit of colloidal silica. This provides a sealant against permeability and capillary action in soils [73]. Reduced hydraulic conductivity can be utilized in preventing water leakage through strata, foundation and underground structures. Nanoparticles are good enough to reduce the plasticity index and crack propagation in the dam embankment [33,61]. Since colloidal silica matrix is highly impermeable, this property of colloidal silica can be utilized in the lining of sanitary landfills to prevent the spread of toxicity to the

nearby unpolluted areas [72].

5. Conclusions

The present article contains the information on fundamentals, mechanisms and benefits of nanoparticles mixed with a variety of soils. After a thorough study, it is concluded that there is a significant gap in the factual reaffirmation and consistency of the results in this area. Though laboratory results showed that just a small amount of nanomaterial can change the soil properties unexpectedly field applications of the research work are barely seen. The astonishing results of nanomaterials are due to their high reactivity. The reactivity has been imparted by their high surface areas and surface charges. Mixing methods of nanoparticles is also a factor for their reactivity. The addition of nanoparticles improved the plastic, strength, and shear hydraulic properties of various soil types if used in optimum quantity. Beyond optimum, the result can get worse. The improved properties have wide applications in pavement construction, water water barriers, embankments, landfilling and water retaining structures. The mechanism of nanomaterials is controlled by the form in which they have been used i.e., to avoid the flocculation of nanomaterials, they must be used in colloidal form rather than powder form.

Future scope

Given the consistent and dependable outcomes generated by nanoclay, it is advisable to promote research endeavours that aim to reduce the utilization of other nanomaterials such as Nanocopper, Nanoalumina, Nanomagnesia, and the like.

It is imperative to ensure that both experimental and numerical studies are aligned with real-world field applications, thereby enhancing the practical relevance of the research.

The integration of systematic and optimization tools should be advocated for further substantiating and validating the optimization processes.

Future research endeavours could yield valuable insights by exploring a diverse array of soil types and various nanomaterials, thereby expanding the scope and depth of our understanding of this field.

Author Contributions

Amit Kumar: Conceptualization and supervision.

Amit Kumar and Kiran Devi: Methodology, Data curation, Original draft preparation, Visualization, Investigation, Paper Writing and Editing.

Conflict of Interest

The authors declare that there is no conflict of interests concerning the publication of this manuscript.

Funding

The authors declare that there is no conflict of interests concerning the financial support of this manuscript.

Acknowledgement

The authors gratefully acknowledge the National Institute of Technology Kurukshetra, Kurukshetra (India), *An Institution of National Importance* and Shree Guru Gobind Singh Tricentenary University, Gurugram for providing the environment for the research work.

Data Availability Statement

The authors declare that [the/all other] data supporting the findings of this study are available within the article [and its supplementary information files].

References

[1] Gupta, A., Rayeen, F., Mishra, R., et al., 2023. Nanotechnology applications in sustainable agriculture: An emerging ecofriendly approach. Plant Nano Biology. 4, 100033. DOI: https://doi.org/10.1016/j.plana.2023.100033

[2] Garg, D., Sridhar, K., Stephen Inbaraj, B., et al., 2023. Nano-biofertilizer formulations for agri-

culture: A systematic review on recent advances and prospective applications. Bioengineering. 10, 1010.
DOI: https://doi.org/10.3390/bioengineering10091010

[3] Sevik, H., Cetin, M., 2015. Effects of water stress on seed germination for select landscape plants. Polish Journal of Environmental Studies. 24, 689-693.
DOI: https://doi.org/10.15244/pjoes/30119

[4] Cetin, M., Adiguzel, F., Kaya, O., 2018. Mapping of bioclimatic comfort for potential planning using GIS in Aydin. Environment, Development and Sustainability. 20, 361-375.
DOI: https://doi.org/10.1007/s10668-016-9885-5

[5] Cetin, M., Sevik, H., Yigit, N., 2018. Climate type-related changes in the leaf micromorphological characters of certain landscape plants. Environmental Monitoring and Assessment. 190, 404.
DOI: https://doi.org/10.1007/s10661-018-6783-3

[6] Yigit, N., Sevik, H., Cetin, M., et al., 2016. Determination of the effect of drought stress on the seed germination in some plant species. Water Stress in Plants. 43, 62.
DOI: https://dx.doi.org/10.5772/63197

[7] Powrie, W., 1997. Soil mechanics: Concepts and application. The University of Sydney: Sydney.

[8] Kulanthaivel, P., Soundara, B., Velmurugan, S., et al., 2021. Experimental investigation on stabilization of clay soil using nano-materials and white cement. Materials Today: Proceedings. 45, 507-511.
DOI: https://doi.org/10.1016/j.matpr.2020.02.107

[9] Mahasneh, B.Z., 2015. Assessment of using cement, Dead Sea sand, and oil shale in treating soft clay soil. European Journal of Scientific Research. 128(4), 245-255.

[10] Gallagher, P.M., Mitchell. J.K., 2002. Influence of colloidal silica grout on liquefaction potential and cyclic undrained behavior of loose sand. Soil Dynamics and Earthquake Engineering. 22, 1017-1026.
DOI: https://doi.org/10.1016/S0267-7261(02)00126-4

[11] Perloff, W.H., 1976. Soil mechanics: Principles and application. John Wiley & Sons: New York.

[12] Hameed, M.Z., Taha, M.R., 2013. A review of stabilization of soils by using nanomaterials. Australian Journal of Basic and Applied Sciences. 7(2), 576-581.

[13] Teizer, J., Venugopal, M., Teizer W., 2012. Nanotechnology and its impact on construction: Bridging the gap between researchers and industry professionals. Journal of Construction Engineering and Management. 138, 594-604.
DOI: https://doi.org/10.1061/(ASCE)CO.1943-7862.0000467

[14] Tiwari, J.N., Tiwari, R.N., Kim, K.S., 2012. Zero-dimensional, one-dimensional, two-dimensional and three-dimensional nanostructured materials for advanced electrochemical energy devices. Progress in Materials Science. 57, 724-803.
DOI: https://doi.org/10.1016/j.pmatsci.2011.08.003

[15] Shevchenko, V.Y., Madison, A.E., 2002. Structure of nanoparticles: II. Magic numbers of zirconia nanoparticles. Glass Physics and Chemistry. 28, 44-49.
DOI: https://doi.org/10.1023/A:1014253514099

[16] Faruqi, M., Castillo, L., Sai, J., 2015. State-of-the-art review of the applications of nanotechnology in pavement materials. Journal of Civil Engineering Research and Practice. 5, 21-27.

[17] Park, C.M., Chu, K.H., Heo, J., 2016. Environmental behavior of engineered nanomaterials in porous media: A review. Journal of Hazardous Materials. 309, 133-150.
DOI: https://doi.org/10.1016/j.jhazmat.2016.02.006

[18] Sun, Y., 2013. Controlled synthesis of colloidal silver nanoparticles in organic solutions: Empirical rules for nucleation engineering. Chemical Society Reviews. 42, 2497-2511.
DOI: https://doi.org/10.1039/C2CS35289C

[19] Selvakumar, S., Kulanthaivel, P., Soundara, B.,

2021. Influence of nano-silica and sodium silicate on the strength characteristics of clay soil. Nanotechnology for Environmental Engineering. 6(46).
DOI: https://doi.org/10.1007/s41204-021-00142-z

[20] Kulanthaivel, P., Selvakumar, S., Soundara, B., et al., 2022. Combined effect of nano-silica and randomly distributed fibers on the strength behavior of clay soil. Nanotechnology for Environmental Engineering. 7(1).
DOI: https://doi.org/10.1007/s41204-021-00176-3

[21] Gallagher, P.M., Lin, Y., 2009. Colloidal silica transport through liquefiable porous media. Journal of Geotechnical and Geoenvironmental Engineering. 135, 1702-1712.
DOI: https://doi.org/10.1061/(ASCE)GT.1943-5606.0000123

[22] Wong, C., Pedrotti, M., El-Mountassir, G., 2018. A study on the mechanical interaction between soil and colloidal silica gel for ground improvement. Engineering Geology. 243, 84-100.
DOI: https://doi.org/10.1016/j.enggeo.2018.06.011

[23] Avadhanulu, M.N., Kshirsagar, P.G.A., 1992. Textbook of engineering physics. S Chand & Company: New Delhi.

[24] Osterwalder, N., Loher, S., Grass, R.N., 2007. Preparation of nano-gypsum from anhydrite nanoparticles: Strongly increased Vickers hardness and formation of calcium sulfate nano-needles. Journal of Nanoparticle Research. 9, 275-281.
DOI: https://doi.org/10.1007/s11051-006-9149-7

[25] Boysen, E., Muir, N.C., Dudley, D., 2011. Nanotechnology for dummies (2nd Ed.). Wiley Publishing Inc.: Hoboken.

[26] Tiwari, A., Mishra, A.K., Kobayashi, H., 2012. Intelligent nanomaterials: Processes, properties, and applications. Scrivener Publishing LLC: Beverly.
DOI: https://doi.org/10.1002/9781118311974

[27] Schwirn, K., Tietjen, L., Beer, I., 2014. Why are nanomaterials different and how can they be appropriately regulated under REACH? Environmental Sciences Europe. 26(1), 1-9.
DOI: https://doi.org/10.1186/2190-4715-26-4

[28] Aricò, A.S., Bruce, P., Scrosati, B., 2010. Nanostructured materials for advanced energy conversion and storage devices. Nature Materials. 4.
DOI: https://doi.org/10.1142/9789814317665_0022

[29] Siddiqui, M.H., Al-Whaibi M.H., 2014. Role of nano-SiO_2 in germination of tomato (Lycopersicum esculentum) seeds. Saudi Journal of Biological Sciences. 21, 13-17.
DOI: https://doi.org/10.1016/j.sjbs.2013.04.005

[30] Ge, Y., Schimel, J.P., Holden, P.A., 2011. Evidence for negative effects of TiO_2 and ZnO nanoparticles on soil bacterial communities. Environmental Science & Technology. 45, 1659-1664.
DOI: https://doi.org/10.1021/es103040t

[31] Gallagher, P.M., Conlee, C.T., Rollins, K.M., 2007. Full-scale field testing of colloidal silica grouting for mitigation of liquefaction risk. Journal of Geotechnical and Geoenvironmental Engineering. 133(2), 186-196.
DOI: https://doi.org/10.1061/(ASCE)1090-0241(2007)133:2(186)

[32] Waalewijn-Kool, P.L., Ortiz, M.D., Van Gestel, C.A.M., 2012. Effect of different spiking procedures on the distribution and toxicity of ZnO nanoparticles in soil. Ecotoxicology. 21, 1797-1804.
DOI: https://doi.org/10.1007/s10646-012-0914-3

[33] Maleki, Y.S., Sharafi, H., 2014. The exploration into the effect of nanoclay additive on soil geotechnical-engineering basic properties. Advances in Environmental Biology. 989-993.

[34] Sarsam, S.I., Husain, A., 2015. Influence of nanomaterials on the microcrack healing of asphalt stabilized subgrade soil. Applied Research Journal. 7, 395-402.

[35] Ng, C.W.W., Coo, J.L., 2015. Hydraulic conductivity of clay mixed with nanomaterials. Canadian Geotechnical Journal. 52, 808-811.

DOI: https://doi.org/10.1139/cgj-2014-0313

[36] Iranpour, B., Haddad, A., 2016. The influence of nanomaterials on collapsible soil treatment. Engineering Geology. 205, 40-53.
DOI: https://doi.org/10.1016/j.enggeo.2016.02.015

[37] Azzam, W.R., 2014. Behavior of modified clay microstructure using polymer nanocomposites technique. Alexandria Engineering Journal. 53, 143-150.
DOI: https://doi.org/10.1016/j.aej.2013.11.010

[38] Changizi, F., Haddad, A., 2016. Effect of Nano-SiO_2 on the geotechnical properties of cohesive soil. Geotechnical and Geological Engineering. 34, 725-733.
DOI: https://doi.org/10.1007/s10706-015-9962-9

[39] Lambe, T.W., Whitman, R.V., 1969. Soil mechanics. Wiley: New York, USA.

[40] Mitchell, J.K., 1993. Fundamentals of soil behavior. John Wiley & Sons: Hoboken.

[41] Shadfan, H., Dixon, J.B., Calhoun, F.G., 1985. Iron oxide properties versus strength of ferruginous crust and iron-glaebules in soils. Soil Science. 140(5), 317-325.
DOI: https://doi.org/10.1097/00010694-198511000-00001

[42] Banadaky, Y.D., Niroumand, H., Kassim, K.A., 2014. A review on various nano imaging systems in geotechnical engineering. Electronic Journal of Geotechnical Engineering. 19, 17333-17344.

[43] Grabar, K.C., Brown K.R., Keating C.D., 1997. Nanoscale characterization of gold colloid monolayers: A comparison of four techniques. Analytical Chemistry. 69, 471-477.
DOI: https://doi.org/10.1021/ac9605962

[44] Taha, M.R., Taha, O.M.E., 2012. Influence of nano-material on the expansive and shrinkage soil behavior. Journal of Nanoparticle Research. 14, 1190.
DOI: https://doi.org/10.1007/s11051-012-1190-0

[45] Majeed, Z.H., Taha, M.R., 2012. Effect of nanomaterial treatment on geotechnical properties of a Penang soft soil. Journal of Asian Scientific Research. 2(11), 587.

[46] Bahari, M., Nikookar, M., Arabani, M., et al. (editors), 2013. Stabilization of silt by nano-clay. 7th National Congress on Civil Engineering; 2013 May 7-8; Zahedan, Iran. p. 7-8.

[47] Nohani, E., Alimakan, E., 2015. The effect of nanoparticles on geotechnical properties of clay. International Journal of Life Sciences. 9, 25-27.
DOI: https://doi.org/10.3126/ijls.v9i4.12670

[48] Priyadharshini, R., Arumairaj, P.D., 2015. Improvement of bearing capacity of soft clay using nanomaterials. International Journal of Scientific Research. 4(6), 218-221.
DOI: https://doi.org/10.36106/IJSR

[49] Hareesh, P., Vinothkumar, R. (editors), 2015. Assessment of nanomaterials on geotechnical properties of clayey soils. International Conference on Engineering Innovations and Solutions (ICEIS-2016); 2016 Apr 25-28; Rome, Italy. p. 66-71.

[50] Ugwu, O.O., Arop, J.B., Nwoji, C.U., 2013. Nanotechnology as a preventive engineering solution to highway infrastructure failures. Journal of Construction Engineering and Management. 139, 987-993.
DOI: https://doi.org/10.1061/(ASCE)CO.1943-7862.0000670

[51] Babu, S., Joseph, S., 2016. Effect of Nano materials on properties of soft soil. International Journal of Science Research. 5, 634-637.

[52] Nasehi, S.A., Uromeihy, A., Nikudel, M.R., 2016. Use of nanoscale zero-valent iron and nanoscale hydrated lime to improve geotechnical properties of gas oil contaminated clay: A comparative study. Environmental Earth Sciences. 75, 733.
DOI: https://doi.org/10.1007/s12665-016-5443-6

[53] Alsharef, J., Taha, M.R., Firoozi, A.A., et al., 2016. Potential of using Nanocarbons to stabilize weak soils. Applied and Environmental Soil Science. 1, 1-9.

DOI: https://doi.org/10.1155/2016/5060531

[54] Osula, D.O.A., 1991. Lime modification of problem laterite. Engineering Geology. 30(2), 141-154.
DOI: https://doi.org/10.1016/0013-7952(91)90040-R

[55] Javadzadeh P., 2019. Investigating the effect of nanomaterials on resistance parameters of clay soil. Journal of Applied Engineering Sciences. 9(22), 2, 139-144.
DOI: https://doi.org/10.2478/jaes-2019-0019

[56] Gelsefidi, S., Alireza, S., 2013. Application of Nanomaterial to Stabilize a Weak Soil [Internet]. International Conference on Case Histories in Geotechnical Engineering. Available from: https://scholarsmine.mst.edu/icchge/7icchge/session_06/5

[57] Changizi, F., Haddad, A., 2017. Improving the geotechnical properties of soft clay with nano-silica particles. Ground Improvement. 170(2), 62-71.
DOI: https://doi.org/10.1680/jgrim.15.00026

[58] Mohammadi, M., Niazian, M., 2013. Investigation of Nano-clay effect on geotechnical properties of Rasht clay. International Journal of Advanced Scientific and Technical Research. 3(3), 37-46.

[59] Nikookar, M., Bahari, M., Nikookar, H. (editors), 2013. The strength characteristics of silty soil stabilized using Nano-Clay. 7th SAS Tech; 2013 Mar 7-8; Bandar-Abbas.

[60] Khalid, N., Arshad, M.F., Mukri, M., 2015. Influence of nano-soil particles in soft soil stabilization. Electronic Journal of Geotechnical Engineering. 20, 731-738.
DOI: https://doi.org/10.1200/JCO.1983.1.2.138

[61] Zahedi, M., Sharifipour, M., Jahanbakhshi, F., 2014. Nanoclay performance on the resistance of clay under freezing cycles. Journal of Applied Sciences and Environmental Management. 18(3), 427-434.
DOI: https://doi.org/10.4314/jasem.v18i3.9

[62] Sharo, A.A., Alawneh, A.S., 2016. Enhancement of the strength and swelling characteristics of expansive clayey soil using nano-clay material. Geo-chicago 2016. 451-457.
DOI: https://doi.org/10.1061/9780784480120.046

[63] Di'az-Rodri'Guez, J.A., Antonio-Izarraras, V.M. (editors), 2004. Mitigation of liquefaction risk using colloidal silica stabilizer. 13th World Conference on Earthquake Engineering; 2004 Aug 1-6; Vancouver, B.C., Canada. p. 1-10.

[64] Moradi, G., Seyedi, S., 2015. Effect of sampling method on strength of stabilized silty sands with colloidal nano silica. Journal of Civil Engineering Research. 5, 129-135.
DOI: https://doi.org/10.5923/j.jce.20150506.01

[65] Persoff, P., Apps, J., Moridis, G.J., 1999. Effect of dilution and contaminants on sand grouted with colloidal silica. Journal of Geotechnical and Geoenvironmental Engineering. 125(6), 461-469.
DOI: https://doi.org/10.1061/(ASCE)1090-0241(1999)125:6(461)

[66] Reginatto, C., Cecchin, I., Carvalho, R.L.R., 2016. Influence of Iron nanoparticle concentration on the hydraulic conductivity of a residual clayey soil. Geo-Chicago 2016.
DOI: https://doi.org/10.1061/9780784480120.047

[67] Bahmani, S.H., Huat, B.B.K, Asadi, A., 2014. Stabilization of residual soil using SiO_2 nanoparticles and cement. Construction and Building Materials. 64, 350-359.
DOI: https://doi.org/10.1016/j.conbuildmat.2014.04.086

[68] Zhang, G., Germaine, J.T., Whittle, A.J., 2003. Effects of Fe-oxide cementation on the deformation characteristics of a weathered old alluvium in San Juan, Puerto Rico. Soils and Foundations. 43(4), 119-130.
DOI: https://doi.org/10.3208/sandf.43.4_119

[69] Khodabandeh, M. A., Nagy, G., Torok, A., 2023. Stabilization of collapsible soils with nanomaterials, fibers, polymers, industrial waste, and microbes: Current trends. Construction and

Building Materials. 368, 130463.
DOI: https://doi.org/10.1016/j.conbuildmat.2023.130463

[70] Bellil, S., Abbeche, K. Bahloul, O., 2018. Treatment of a collapsible soil using a bentonite–cement mixture. Studia Geotechnica et Mechanica. 40(4), 233-243.
DOI: https://doi.org/10.2478/sgem-2018-0042

[71] Zhang, G., 2007. Soil nanoparticles and their influence on the engineering properties of soils. Geo-Denver. 1-13.
DOI: https://doi.org/10.1061/40917(236)37

[72] Gallagher, P.M., Pamuk, A., Abdoun T., 2007. Stabilization of liquefiable soils using colloidal silica grout. Journal of Materials in Civil Engineering. 19, 33-40.
DOI: https://doi.org/10.1061/(ASCE)0899-1561(2007)19:1(33)

[73] Gallagher, P.M., 2000. Passive site remediation for mitigation of liquefaction risk [Ph.D. thesis]. Blacksburg, VA: Virginia Polytechnic Institute and State University.

BILINGUAL PUBLISHING GROUP

Journal of Building Material Science

https://journals.bilpubgroup.com/index.php/jbms

ARTICLE

Unveiling the Carbonation Behavior and Microstructural Changes of Magnesium Slag at 0 °C

***Junhao Ye*[1], *Songhui Liu*[1*], *Jingrui Fang*[2], *Xuemao Guan*[1], *Hui Guo*[1]**

[1] *Henan Key Laboratory of Materials on Deep-Earth Engineering, School of Materials Science and Engineering, Henan Polytechnic University, Jiaozuo, Henan, 454003, China*

[2] *State Key Laboratory of Green Building Materials, China Building Materials Academy, Beijing, 100024, China*

ABSTRACT

Magnesium slag (MS) is an industrial byproduct with high CO_2 sequestration potential. This study investigates the carbonation behavior and microstructural changes of MS during wet carbonation at 0 °C. XRD, TG, FTIR, SEM, and BET techniques were used to characterize the phase composition, microstructure, and porosity of MS samples carbonated for different durations. The results showed that the main carbonation products were calcite, vaterite, and highly polymerized silica gel, with particle sizes around 1 μm. The low-temperature environment retarded the carbonation reaction rate and affected the morphology and crystallization of calcium carbonate. After 480 min of carbonation, the specific surface area and porosity of MS increased substantially by 740% and 144.6%, respectively, indicating improved reactivity. The microstructure of carbonated MS became denser with calcite particles surrounded by silica gel. This study demonstrates that wet carbonation of MS at 0 °C significantly enhances its properties, creating an ultrafine supplementary cementitious material with considerable CO_2 sequestration capacity.

Keywords: Wet carbonation; Ultrafine supplementary cementitious materials; Calcium carbonate; Magnesium slag

1. Introduction

With the rapid development of modern industry, anthropogenic carbon dioxide (CO_2) emissions have been exponentially increasing, posing a significant threat to the environment [1]. The cement industry, as a pillar of infrastructure development, is responsible

*CORRESPONDING AUTHOR:
Songhui Liu, Henan Key Laboratory of Materials on Deep-Earth Engineering, School of Materials Science and Engineering, Henan Polytechnic University, Jiaozuo, Henan, 454003, China; Email: liusonghui@hpu.edu.cn

ARTICLE INFO
Received: 19 November 2023 | Revised: 11 December 2023 | Accepted: 20 December 2023 | Published Online: 27 December 2023
DOI: https://doi.org/10.30564/jbms.v5i2.6092

CITATION
Ye, J.H., Liu, S.H., Fang, J.R., et al., 2023. Unveiling the Carbonation Behavior and Microstructural Changes of Magnesium Slag at 0 °C. Journal of Building Material Science. 5(2): 37-50. DOI: https://doi.org/10.30564/jbms.v5i2.6092

COPYRIGHT
Copyright © 2023 by the author(s). Published by Bilingual Publishing Group. This is an open access article under the Creative Commons Attribution-NonCommercial 4.0 International (CC BY-NC 4.0) License. (https://creativecommons.org/licenses/by-nc/4.0/).

for approximately 7% of global CO_2 emissions [2]. The production of traditional Portland cement not only consumes massive amounts of raw materials and energy but also releases enormous amounts of CO_2 [3-5]. It is estimated that for every ton of Portland cement produced, approximately 0.8-1.0 tons of CO_2 are emitted. Consequently, developing alternative cementitious materials with low carbon footprints and CO_2 sequestration capacities has become an urgent need.

In recent years, mineral carbonation has emerged as a promising approach for reducing CO_2 emissions in the cement and construction sector [6-10]. This process chemically binds CO_2 with calcium or magnesium-rich materials to form stable carbonates, providing a route for permanent CO_2 sequestration [11-13]. Simultaneously, the carbonation reaction can produce supplementary cementitious materials (SCMs) with enhanced properties and reactivity [14,15]. Multiple industrial alkaline wastes and byproducts with high calcium or magnesium contents such as steel slags, power plant ashes, and magnesium slags have been identified as suitable precursors for mineral carbonation [16-20]. Compared to natural minerals, these artificial calcium/magnesium-rich solid wastes not only possess higher reactivity and faster carbonation kinetics but also allow for the recycling of industrial byproducts, enabling the realization of a cyclic economy [21-24].

Among various mineral carbonation options, the carbonation of magnesium slag has attracted increasing interest in recent years [25]. Magnesium slag is a byproduct of magnesium smelting processes, primarily consisting of calcium oxide (CaO), silicon dioxide (SiO_2), and magnesium oxide (MgO). With the dramatic growth in magnesium production, driven by strong market demand, China has become the world's largest magnesium producer, accounting for approximately 90% of the global output. Consequently, vast quantities of magnesium slag are being generated. Current estimates indicate an annual magnesium slag output of over 6 million tons in China. Despite its chemical composition rich in oxides, magnesium slag has found limited large-scale utilization due to issues such as low activity, poor stability, and potential expansion [26]. Landfilling has been the primary disposal route, leading to serious environmental problems and waste of resources.

The predominant mineral phase of magnesium slag is dicalcium silicate (C_2S), which exhibits high susceptibility to carbonation reactions [27-30]. Studies have confirmed that carbonation can effectively stimulate the hydration reactivity of C_2S while mitigating the expansion issues associated with magnesium slag [26]. Both dry and wet carbonation processes have been shown to improve the properties and activity of magnesium slag, transforming it into a viable SCM. Carbonated magnesium slag displays enhanced hydration activity, reduced CaO expansion, increased strength, and self-cementing characteristics when used as concrete admixtures. Moreover, accelerated carbonation curing has been successfully implemented to synthesize magnesium slag-based cementitious materials, with compressive strengths exceeding 100 MPa in some studies [31]. Evidently, carbonation provides an efficient technique to stabilize magnesium slag and unlock its latent hydraulic properties.

However, the carbonation of magnesium slag is a complex physicochemical process influenced by several parameters including CO_2 concentration, temperature, relative humidity, liquid/solid ratio, and pressure [26,32]. In particular, temperature plays a crucial role in shaping the carbonation reaction kinetics and the composition of reaction products [33]. Most studies have focused on investigating the effects of room temperature and elevated temperatures on the carbonation process [25]. Far fewer efforts have explored the implications of conducting carbonation under low-temperature conditions.

It is well established that temperature has a significant impact on the solubility of CO_2 as well as the dissolution kinetics of Ca^{2+} and Mg^{2+} ions, consequently affecting $CaCO_3$ crystallization and growth [34,35]. Lower temperatures lead to reduced CO_2 diffusion rates in the aqueous phase and hinder the dissolution of Ca^{2+} and Mg^{2+}, which directly controls the kinetics of calcium carbonate precipitation. Moreover, temperature influences the polymorphs

and morphology of the formed calcium carbonate crystals [36]. The effects of temperature on the carbonation reaction pathways and products are complex and remain incompletely understood.

Elucidating the implications of low-temperature carbonation on magnesium slag is important from both a scientific perspective, in terms of revealing the underlying mechanisms, as well as a practical viewpoint, in terms of assessing its potential for mitigating CO_2. Nevertheless, current literature lacks comprehensive investigations analyzing the phase transformations, microstructural changes, and CO_2 sequestration efficiency of magnesium slag undergoing carbonation specifically under low-temperature conditions. Most studies focus on room temperature or use elevated temperatures to accelerate the carbonation reactions. The carbonation behavior of magnesium slag at temperatures closer to natural conditions remains relatively unclear.

Therefore, this paper aims to conduct a detailed assessment of the effects of wet carbonation at 0 °C on the physiochemical characteristics of magnesium slag. The evolution of the phase composition at different carbonation conversion levels and its impacts on the microstructure, morphology, specific surface area, and porosity of magnesium slag will be analyzed using a suite of characterization techniques. The findings are expected to provide new insights into the implications of low-temperature environments on the carbonation mechanisms of magnesium slag. Furthermore, the results will allow evaluation of the CO_2 sequestration potential and the prospective utilization of magnesium slag as an SCM following low-temperature carbonation treatment.

2. Experimental program

2.1 Raw materials

The magnesium slag (MS) utilized in this study was acquired from Yulin City, Shanxi Province, China, employing the Pidgeon method. Deionized water sourced from the laboratory was employed as the solvent. The chemical composition of the magnesium slag and its particle size distribution are detailed in **Table 1** and **Figure 1**, respectively. The XRD of MS is shown in **Figure 2**.

Upon reviewing the data presented in **Table 1**, it is evident that the primary chemical constituents of MS are CaO, SiO_2, and MgO. Numerous studies have demonstrated that the elevated MgO content can result in later-stage matrix hydration expansion, thereby constraining the widespread utilization of MS [25,26]. However, the high content of Ca and Mg has very high carbonation activity, indicating that Pidgeon process magnesium slag does have great potential to sequester carbon dioxide.

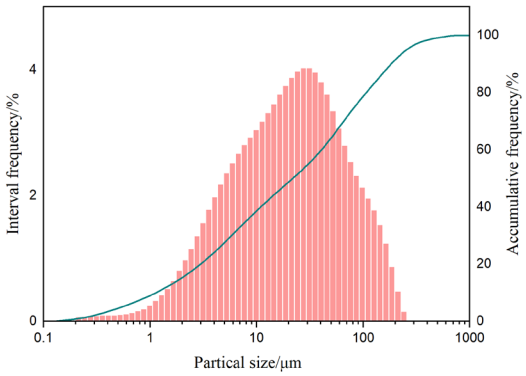

Figure 1. The particle size distribution of MS.

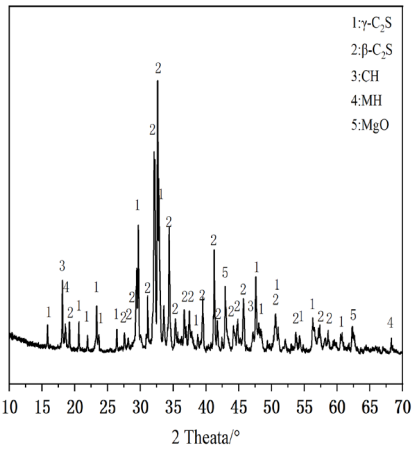

Figure 2. The XRD of MS.

Table 1. Chemical composition of MS.

Oxide	SiO_2	Al_2O_3	CaO	Fe_2O_3	MgO	Others
MS	29.88	1.06	50.98	3.52	11.27	3.29

2.2 The carbonation of MS

The carbonation of MS is shown in **Figure 3**. First,

the dried MS powder and chilled deionized water were weighed in the ratio of 1:40. Then, the suspension of MS and deionized water was placed into a large beaker containing ice cubes (size 10 × 10 × 10 mm^3) and cold deionized water. The speed of the stirring device was set to 400 r/min. To further dissolve the MS, the suspension was stirred for 10 min, and then carbon dioxide was injected into the suspension at a rate of 0.1 L/min/5 g of MS. Carbon dioxide was purchased from Gas Commerce at a concentration higher than 99.9%. The temperature of the MS suspension was monitored in real-time throughout the carbonation process using a temperature sensor. The temperature of the mass spectrometry suspension was maintained at around 0 °C by adjusting the amount of ice in the large beaker. Subsequently, the mass spectrometry suspensions of different carbonation times were vacuum filtered and the resulting samples were washed with anhydrous ethanol. This was done to ensure that the samples stopped hydrating and to facilitate drying. Finally, the samples were dried in a vacuum oven at 50 °C to obtain MS samples with different degrees of carbonation. The carbonated MS samples were named C-MS.

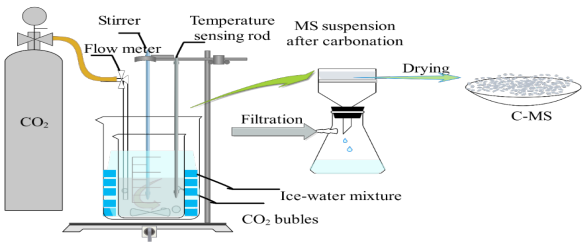

Figure 3. Preparation of C-MS powder samples.

2.3 Testing methods

X-ray diffractometer

The mineralogical composition of the samples was determined using an X-ray diffractometer equipped with a copper target (Rigaku, Tokyo, Japan). The test instrument utilizes an accelerating voltage of 45 kV and a current of 200 mA during the test. In addition, the instrument is set to analyze in 0.02 steps.

Thermal analysis

The comprehensive thermal analyzer (BJ-HCT-3) used in this study was produced by Beijing Hengjiu Scientific Instrument Factory. Before the test begins, the powder sample is weighed and placed on a sample stage. The instrument temperature is raised from room temperature to 1000 °C at a rate of 10 °C/min.

Fourier transform spectra (FTIR)

To further examine the development of the silicon phase present in the samples, an analysis was conducted using Fourier transform spectroscopy employing the solid powder total reflection method. The testing instrument employed was a fully automated switching Fourier transform spectrometer model V70, covering a range of 400 to 4000 cm^{-1} [25]. All powdered specimens were maintained in a dry and ground state for the analysis.

To further explore the ratio change of silica gel and C-S-H gel under different carbonation conditions, the spectrum between 1000 and 1200 cm^{-1} was deconvolved using Origin Pro software. According to the peak range of silica gel and C-S-H, the position of the target peak was determined, and the original curve was divided into C-S-H peak and silica gel peak, to clarify the process of MS carbonation products at low temperatures.

Scanning electron microscope (SEM)

Scanning electron microscope (SEM) images of the powder samples were obtained using a Merlin SEM in high vacuum mode at an accelerating voltage of 15 kV. To enhance conductivity, all samples were coated with a thin layer of gold.

Pore structure

In studying the evolution of pore structure in C-MS under varying degrees of carbonation, the TriStar II 3020BET tester from Micromeritics was employed [37]. The examination centered on assessing alterations in the total specific surface area and pore volume of the samples. Before the analysis, a degassing procedure was carried out on the samples at a temperature of 45 °C for 6 hours to eliminate any remaining moisture and gaseous impurities.

3. Results and discussion

3.1 Carbonation degree

Figure 4 depicts the TG-DTG curves of MS

with varying degrees of carbonation. A total of four different weight loss peaks can be seen in the DTG results. First, the weight loss peak near 100 °C is the loss of mass due to the evaporation of bound water from the amorphous gel in the sample. It is interesting to note that after 480 minutes of carbonation, the peak weight loss is highest at 100 °C, indicating that the largest amount of gel was produced at this time. The weight loss peak observed in the temperature range of 400-450 °C is attributed to the mass loss resulting from the thermal decomposition of calcium hydroxide ($Ca(OH)_2$), a hydration product, at high temperatures [38,39]. The weight loss peak observed in the temperature range of 500-600 °C is attributed to the de-carbonation processes of amorphous calcium carbonate (ACC) and poorly crystalline vaterite [40]. Furthermore, the weight loss peak observed between 700-800 °C is caused by the high-temperature decomposition of calcite [41]. Notably, this peak exhibits an increasing trend and gradually shifts to higher temperatures with prolonged carbonation.

The calcium carbonate content under various carbonation conditions was determined using Equation (1), while Equations (2)-(4) were utilized to calculate the degree of carbonation of MS at different carbonation times under an ambient temperature of 0 °C [42].

$$Cc(\%) = \frac{Cc_{CO_2} \times \left(\frac{100}{44}\right)}{M_{900°C}} * 100\% \quad (1)$$

$$\partial = \frac{CO_{2uptake.actual}}{CO_{2uptake.max}} \quad (2)$$

$$CO_{2uptake.actual} = \left(\frac{Cc_{CO_2}}{M_{900°C}}\right) \quad (3)$$

$$CO_{2uptake.max} = \left(\frac{M_{CO_2}}{M_{CaO}}\right) * [CaO + (1.09MgO)] \quad (4)$$

The CO_2 bound in $CaCO_3$ (550-850 °C) is represented by Cc_{CO2}, while $M_{900°C}$ denotes the residual mass at 900 °C. Additionally, M_{CO2} and M_{CaO} refer to the molecular weights of CO_2 and CaO, respectively. The MgO content of cement can be found in **Table 1**. The calculation results are shown in **Table 2**.

Figure 5 illustrates the variation of carbonation degree in MS at different carbonation times. The process can be divided into three stages. Firstly, during the initial ten minutes of carbonation reaction, the carbonation degree of MS increases from an initial 6% to 40%. In this stage, the dissolution rate of CO_2 in water becomes the determining factor. Subsequently, the carbonation reaction enters the second stage, where the carbonation process of MS is influenced by the dissolution and transfer rate of minerals and Ca^{2+} [42]. Compared to the first stage, the rate of carbonation degree advancement in MS slows down, with only a 30% increase after 50 minutes. As the carbonation reaction progresses to the third stage, the continuous low-temperature environment restricts the diffusion of CO_2 and the migration of Ca^{2+}, significantly prolonging the reactivity of the carbonation process [35,42]. It takes 480 minutes for the carbonation degree of MS to reach 80%.

From the above results, it can be observed that even when the carbonation reaction of MS continues in a low-temperature environment, the early-stage reactivity is primarily influenced by the dissolution of CO_2 and the migration of Ca^{2+}. It is not until the later stage of the carbonation reaction that the continuous low temperature imposes restrictive effects on the carbonation process in MS.

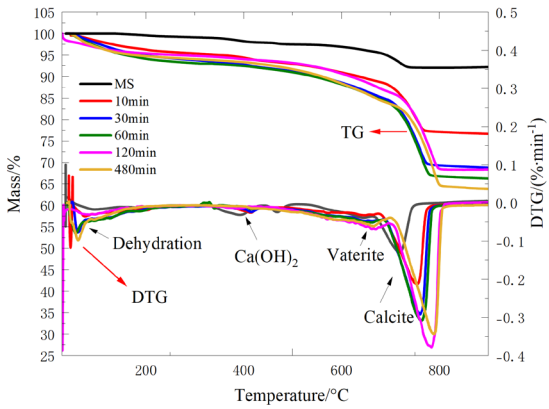

Figure 4. TG-DTG curves of MS with different carbonation times.

Table 2. The calculation results of MS under different carbonation times.

Time/min	Cc_{CO2}/%	CC%	α/%
0	5.30	13.07	6.8
10	15.23	45.18	40.11
30	21.25	70.16	61.72
60	23.40	80.35	70.55
120	23.91	79.52	70.57
480	26.22	93.30	83.23

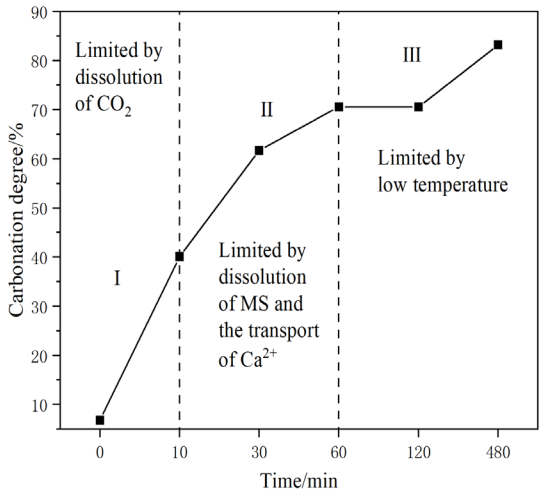

Figure 5. Carbonation degree of MS with different carbonation times.

3.2 Phase composition

Figure 6 presents the XRD analysis of MS with different carbonation times under low-temperature conditions. In **Figure 6**, it is observed that the predominant carbonation product of MS at low temperatures is calcite. The position of the calcite diffraction peak remains relatively unchanged with increasing carbonation time, but its intensity increases, leading to a weakening of the C_2S diffraction peak. This phenomenon arises from the continuous injection of carbon dioxide, which dissolves in water, generating carbonic acid. The carbonic acid subsequently reacts with the dissolved Ca^{2+} ions present in the mineral suspension, resulting in the precipitation of calcite. Consequently, the presence of calcite leads to an observable increase in the diffraction peak associated with its crystal structure. Additionally, faint calcite diffraction peaks are also noticeable in the XRD curves of the uncarbonated MS, indicating a minor carbonation reaction of the material.

According to the XRD results, the main carbonated products of MS were not affected under prolonged low-temperature conditions. In the early stage of the carbonation reaction (10-30 minutes), the diffraction peak of the C_2S mineral gradually weakened, while the diffraction peak belonging to calcite gradually increased, and a weak peak of vaterite also appeared. This indicates that temperature does not have a significant influence on the products in the early stage of wet carbonation, and the post-carbonated products of MS still exist predominantly in the crystalline form of calcite. As the carbonation reaction enters the intermediate stage (30-60 minutes), the number of calcite diffraction peaks increases and the peak intensity gradually increases, while the vaterite diffraction peak becomes more pronounced. With the extension of carbonation time, the diffraction peak of C_2S eventually disappears. When the carbonation time reaches 480 minutes, the peak intensity of calcite reaches its maximum. These results show that the early stage (30 min) of the carbonation reaction at a low temperature helps to stabilize the crystal structure of vaterite, but as the carbonation reaction continues, the vaterite transforms into calcite.

Numerous studies have shown that the crystal forms of calcium carbonate are mainly divided into three types, namely calcite, aragonite, and vaterite, in the order of increasing stability. Among them, vaterite easily transforms into calcite in aqueous solutions. From the results in **Figure 6**, it can be observed that the low-temperature environment contributes to stabilizing the crystal structure of vaterite. This phenomenon can be attributed to the fact that low temperature restricts the diffusion of CO_2 gas in the aqueous solution and the migration of Ca^{2+}, thereby impeding the transformation process of vaterite to calcite and allowing vaterite to exist stably [35].

3.3 Evolution of Si

Figure 7 displays the FTIR spectra, revealing absorption bands associated with ACC (amorphous calcium carbonate) and calcite. Based on the results, a total of four vibrational peaks were observed. Specifically, the peaks observed at 1417 cm^{-1} and 712 cm^{-1} correspond to the asymmetric stretching vibration (υ^3) and in-plane bending vibration (υ^2) of the C-O bond, respectively [43]. Additionally, the peak at 868 cm^{-1}

represents the out-of-plane bending vibration (υ^4) of the C-O bond. These findings once again confirm the presence of carbonates. It is noteworthy that the vibrational peaks observed in the wavenumber range of 993-1066 cm^{-1} represent the vibration of the Si-O bond (υ^3). This indicates that after undergoing carbonation at 0 °C, the silicon in MS exists in the form of highly polymerized silica gel.

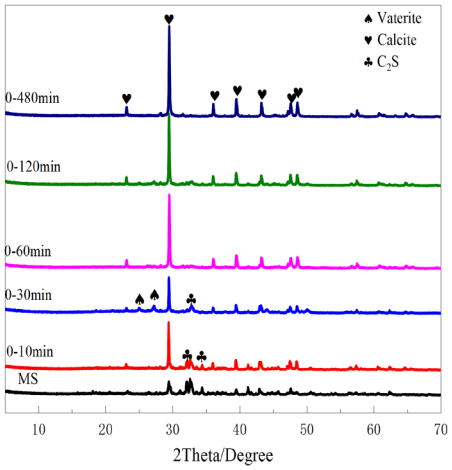

Figure 6. XRD analysis of MS with different carbonation times under low-temperature conditions.

Similar to the XRD results, faint vibrational peaks related to calcite are observed in the FTIR analysis of the uncarbonated MS, providing further evidence of slight carbonation. With the progression of the reaction, an increase in the amount of calcite is observed. Notably, the vibrational peak of the Si-O bond shifts to a higher wave number (1066 cm^{-1}), indicating an enhanced degree of polymerization of the silica-oxygen tetrahedra and the formation of highly polymerized silica gel. This transition becomes more apparent after 30 minutes of carbonation, consistent with our previous findings suggesting a significant enhancement in the degree of polymerization of gel products generated from MS, both at room temperature and under low-temperature conditions.

To gain a better understanding of the evolution of silicon dioxide phase structures in MS during carbonation, the vibrational peaks between 800 cm^{-1} and 1200 cm^{-1} were analyzed for samples with different carbonation times (As shown in **Figure 8**). Previous studies have demonstrated the feasibility of using FTIR analysis to determine the levels of unhydrated phases, hydrated calcium silicate gel (C-S-H), and silica gel [42]. The fitting results are shown in **Table 3**.

The results indicate that during carbonation reactions conducted in a low-temperature environment, prior to 30 minutes of carbonation time, decalcification of hydrated calcium silicate gel and an increase in silica gel content were observed. As the carbonation reaction continued for 120 minutes, further decalcification of hydrated calcium silicate gel occurred, leading to its conversion into silica gel and resulting in an increased silica gel content.

These findings reveal that a sustained low-temperature environment does not significantly influence the transformation of early gel products during the carbonation of MS. After 120 minutes, although the continuous low-temperature environment limits the diffusion of CO_2 and the migration of Ca^{2+}, it actually facilitates the inward progress of the carbonation reaction, thereby increasing the degree of carbonation and the silica gel content within the matrix [35].

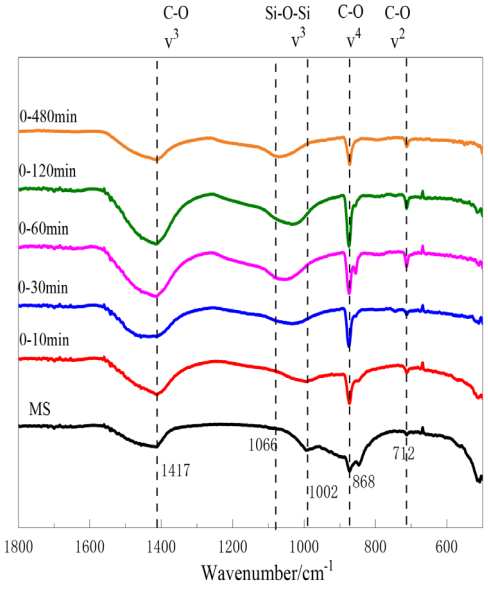

Figure 7. FTIR analysis of MS with different carbonation times under low-temperature conditions.

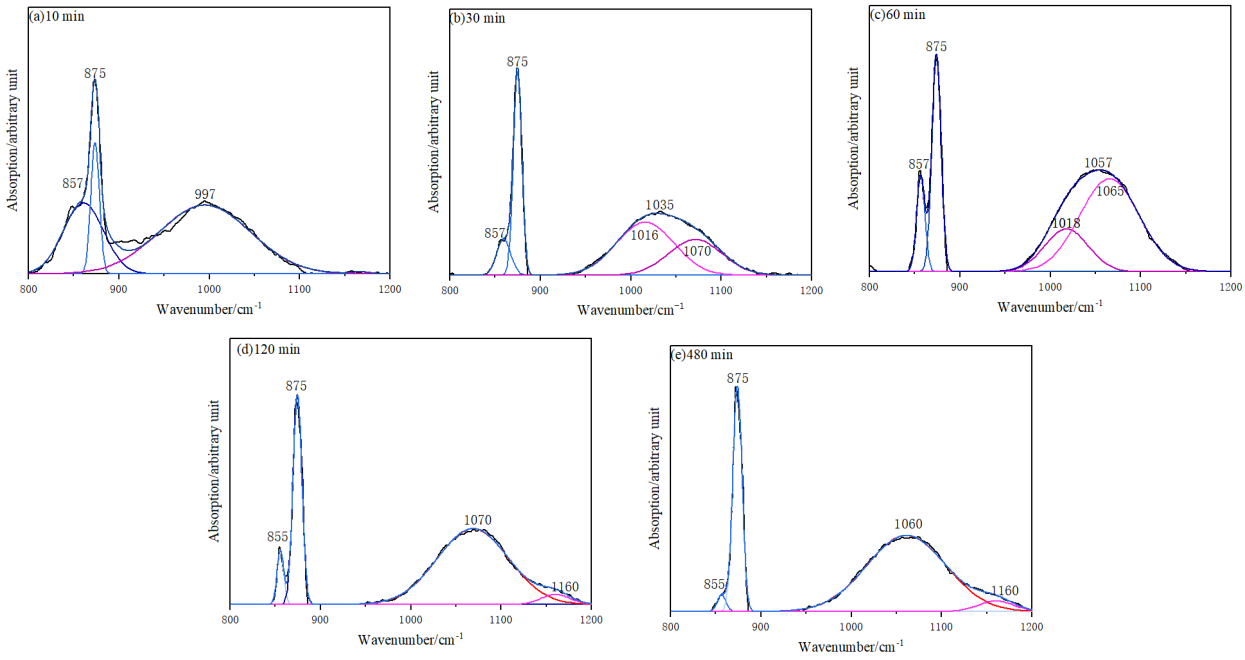

Figure 8. The resolving of the overlapping peak of FTIR spectra between 800 and 1200 cm^{-1} of carbonated MS samples at different carbonation conditions (a) 10 min, (b) 30 min, (c) 60 min, (d) 120 min and (e) 480 min.

Table 3. The deconvolution results of FTIR curves between 800 and 1200 cm^{-1} (%).

Time/min	Unhydrated phases	C-S-H gel	Silica gel
10	30.91%	68.73%	0.36%
30	9.25%	55.66%	35.09%
60	11.86%	22.71%	65.43%
120	8.08%	0	91.92%
480	5.31%	0	94.69%

3.4 Microstructure of C-MS

SEM

Figure 9 presents the SEM-EDS images of C-MS. By comparing the microscopic morphology of MS with different carbonation degrees, several important observations can be made.

In just 10 minutes, the carbonation reaction yields calcite with distinct morphology, indicating the rapid nature of the carbonation process even at low temperatures. At 30 minutes, ACC gradually transforms into vaterite. At this point, most of the calcite and vaterite are 0.8 μm in size, with only a few vaterites reaching 1.5 μm in diameter. In addition, small-sized calcite particles begin to aggregate, forming rhombic massive calcite structures with a large number of vaterite particles and gel products attached. The produced calcite and vaterite particles have sizes not exceeding 1 μm. As the carbonation reaction progresses (between 60-120 minutes), the calcite particles become tightly surrounded by a significant amount of gel products. This phenomenon becomes even more pronounced at the 480-minute.

Compared to previous studies, when wet carbonation of MS is conducted at room temperature, the resulting calcium carbonate exists in the forms of calcite and aragonite, with calcite being dominant. However, under low-temperature conditions, the aragonite form of calcium carbonate disappears, and a larger quantity of vaterite appears. Additionally, from **Figure 9(b)**, it can be observed that the calcite formed under low-temperature conditions adopts a cubic structure, while vaterite has a more complete

spherical shape. The reason for this phenomenon is that prolonged low-temperature conditions restrict the diffusion rate of CO_2 gas in the aqueous solution, but promote internal carbonation, resulting in more complete carbonation of the matrix and complete growth of calcite crystals. Furthermore, low temperature hinders the migration of Ca^{2+} dissolved from minerals like C_2S, limiting the nucleation process of calcium carbonate and the transformation of vaterite into calcite. As a result, the layered calcite structure disappears, and well-formed cubic calcite crystals emerge.

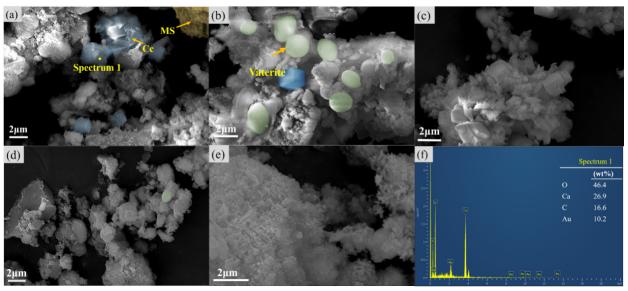

Figure 9. SEM-EDS images of C-MS: (a) 10 min; (b) 30 min; (c) 60 min; (d) 120 min; (e) 480 min; (f) EDS of the spectrum.

BET surface area and pore structure

To investigate the changes in MS pore structure under low-temperature conditions at different degrees of carbonation, the BET analysis method was employed in this study. **Figures 10(a) and 10(b)** present the N_2 adsorption isotherm plots and pore volume distribution of MS with varying degrees of carbonation. **Figure 10(a)** reveals a significant increase in nitrogen uptake when the carbonation time reaches 30 minutes and the relative pressure ranges from 0.7 to 1. The uptake experiences a sharp increase at 120 minutes, accompanied by an expanded relative pressure range. Additionally, **Figure 10(b)** provides further insights into the pore size distribution of MS.

The BET test results of MS with different carbonation degrees are listed in **Table 4**. From the results, it can be seen that the hole volume and specific surface area of MS gradually increase with the increase of carbonation degree. However, there is a slight decrease in specific surface area at 10 and 60 minutes. A comparison of MS test results before and after 120 minutes of carbonation showed a significant increase in the cumulative pore volume, from 0.024245 cm^3/g to 0.047098 cm^3/g. This observed increase can be attributed to the continued dissolution of minerals present in the MS during the decalcification process, especially C_2S. As a result, a significant change in the phase composition of the MS occurs, leading to an increase in the pore volume. In addition, **Figure 10(b)** shows a clear trend of increasing volume of pores larger than 25 nm as well as gel pores smaller than 25 nm. This trend can be attributed to the formation of van der Waals and hydrogen bonds during carbonation [37]. Consequently, this leads to an increase in the number of small particles and pores, which ultimately results in an overall increase in pore volume.

Based on our previous study and the FTIR analysis results (**Figure 7**), it is evident that gel polymerization begins after 30 minutes of carbonation. Consistently, the BET test results of MS also reveal an elevation in pore volume by approximately 73.7% after 30 minutes compared to uncarbonated MS. This can be attributed to the continuous dissolution of Ca^{2+}, which generates numerous fine pores and leads to the observed increase. After 480 min, it was found from the results that the specific surface area of MS increased by 740% and the pore volume increased by 144.6% compared with that before carbonation, which indicated a significant increase in the activity and specific surface area of MS during the low-temperature carbonation process.

3.5 Growth mechanism of CaCO3 under a low-temperature environment

This study investigates the carbonation behavior of MS at varying degrees under a low-temperature environment using XRD, TG, FTIR, BET, and SEM-EDS analysis. Based on the results of the above tests, it can be observed that the main carbonation products resulting from wet carbonation of MS at 0 °C are calcite and highly polymerized silica gel. **Figure 11** illustrates the evolution of $CaCO_3$ growth at low temperatures.

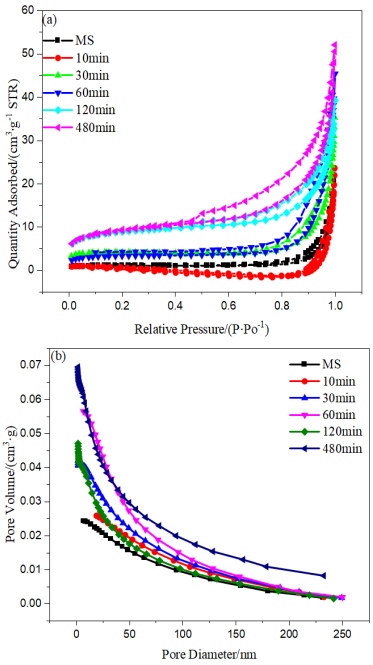

Figure 10. BET curves of MS with different degrees of carbonation.

Table 4. BET test results of MS with different degrees of carbonation.

Different time (min)	Specific surface area (m^2/g)	Hole volume (cm^3/g)
MS	3.5305	0.024245
10 min	1.1851	0.025903
30 min	12.8038	0.042108
60 min	10.4350	0.056580
120 min	28.9021	0.047098
480 min	29.6573	0.059295

In the initial stage (0-30 min), the carbonation reaction occurs rapidly, leading to the conversion of ACC into calcite. Calcite particles rapidly increase in size, while a small amount of silica-gel forms around them. Subsequently, after 30 minutes, the reaction enters the stabilization stage, and calcite decomposes into clusters of poorly crystallized and lumpy calcite due to cracking. The persistent low-temperature environment restricts the diffusion rate of CO_2 and the dissolution of Ca^{2+} and Mg^{2+}, thereby influencing the growth of calcite crystals. Additionally, vaterite, derived from ACC, surrounds the calcite particles. In the final stage of the reaction, the low-temperature environment further hinders the growth rate of calcite particles, leading to the appearance of a gel layer on their surface.

The primary mineral component of MS, C_2S, is subject to various influential factors including Ca^{2+} ion concentration, ion leaching rate, and solution pH. These factors play a crucial role in determining the nucleation and growth processes of calcium carbonate. Compared to our previous studies on room-temperature wet carbonation, the main carbonation products observed at low temperatures consist of calcite crystals and highly polymerized gel structures, with significant gel polymerization occurring only at the 30-minute mark [25]. Notably, in contrast to the appearance of small amounts of aragonite in the carbonation products at room temperature, the low-temperature carbonation process does not generate aragonite, but rather small vaterite. Furthermore, it is worth noting that the amount of calcium carbonate generated during the same time frame at room temperature exhibits a substantial increase compared to that produced during low-temperature wet carbonation. This disparity suggests that the low-temperature environment significantly retards the rate of the carbonation reaction. Furthermore, the microscopic morphology of calcite at room temperature reveals a laminar accumulation with a small amount of aragonite and gel surrounding it, while calcite clusters generated at low temperatures exhibit a substantial presence of gel layers around them. In this study, the low-temperature carbonation process significantly limits the dissolution rate of Ca^{2+} ions, resulting in a lower concentration of Ca^{2+} ions in the MS suspension and a reduced carbonation rate for the corresponding minerals [35]. As a result, the production and size growth of calcite-type calcium carbonate is constrained.

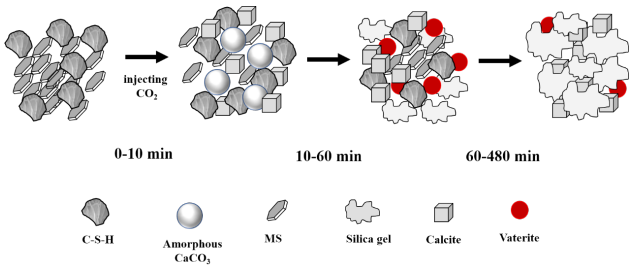

Figure 11. Evolution of $CaCO_3$ growth in a low-temperature environment.

4. Conclusions

This study investigated the carbonation behavior and microstructural changes of magnesium slag undergoing wet carbonation at 0 °C through a comprehensive set of characterization techniques. The following conclusions can be drawn:

(1) The predominant carbonation products are calcite, vaterite, and highly polymerized silica gel, with particle sizes around 1 μm. The persistent low-temperature environment affects the morphology and crystallization of calcium carbonate, slowing down the reaction kinetics.

(2) As carbonation progresses, a layer of silica gel envelops the surfaces of the formed calcium carbonate particles. The low temperature restricts the dissolution of Ca^{2+} ions, limiting the growth of calcite crystals.

(3) After 480 min of carbonation, the specific surface area and porosity of magnesium slag increased remarkably by 740% and 144.6%, respectively, indicating significantly improved reactivity and ultrafine particle size distribution

(4) The microstructure of carbonated magnesium slag became denser, with calcite particles intimately surrounded by the silica gel phase, due to the low temperature impeding crystal growth.

(5) Wet carbonation treatment at 0 °C can effectively transform magnesium slag into an ultrafine supplementary cementitious material with high CO_2 sequestration capacity.

Overall, this study provides new insights into the effects of low-temperature carbonation environments on the physicochemical characteristics of magnesium slag. The results demonstrate that wet carbonation at 0 °C significantly enhances the properties of magnesium slag, creating a high reactivity SCM product with major implications for reducing the carbon footprint of the cement and construction industry. Further research can build on these findings to optimize the synthesis conditions and expand the utility of carbonated magnesium slag.

Conflict of Interest

There is no conflict of interest.

Data Availability Statement

Data will be made available on request.

Acknowledgement

The authors appreciate the support from the National Key R & D Program Intergovernmental International Science and Technology Innovation Cooperation Project (2018YFE0107300), the China Building Materials Federation (20221JBGS03-11), the Science and Technology Project of Henan Province (211110231400, 212102310559, 212102310564, 222300420167, 22A430022), the Opening Project of the State Key Laboratory of Green Building Materials (2021GBM06), the Henan Outstanding Foreign Scientists' Workroom (GZS2021003).

References

[1] Zajac, M., Song, J., Ullrich, P., et al., 2024. High early pozzolanic reactivity of alumina-silica gel: A study of the hydration of composite cements with carbonated recycled concrete paste. Cement and Concrete Research. 175, 107345. DOI: https://doi.org/10.1016/j.cemconres.2023.107345

[2] Liu, Z., Lv, C., Wang, F., et al., 2023. Recent advances in carbonatable binders. Cement and Concrete Research. 173, 107286. DOI: https://doi.org/10.1016/j.cemconres.2023.107286

[3] Poon, C.S., Shen, P., Jiang, Y., et al., 2023. Total recycling of concrete waste using accelerated carbonation: A review. Cement and Concrete Research. 173, 107284. DOI: https://doi.org/10.1016/j.cemconres.2023.107284

[4] Cui, K., Lau, D., Zhang, Y., et al., 2021. Mechanical properties and mechanism of nano-Ca-

CO_3 enhanced sulphoaluminate cement-based reactive powder concrete. Construction and Building Materials. 309, 125099.
DOI: https://doi.org/10.1016/j.conbuildmat.2021.125099

[5] Shang, D., Wang, M., Xia, Z., et al., 2017. Incorporation mechanism of titanium in Portland cement clinker and its effects on hydration properties. Construction and Building Materials. 146, 344-349.
DOI: https://doi.org/10.1016/j.conbuildmat.2017.03.129

[6] Mao, Y., Drissi, S., He, P., et al., 2024. Quantifying the effects of wet carbonated recycled cement paste powder on the properties of cement paste. Cement and Concrete Research. 175, 107381.
DOI: https://doi.org/10.1016/j.cemconres.2023.107381

[7] Jiang, Y., Li, L., Lu, J.X., et al., 2022. Mechanism of carbonating recycled concrete fines in aqueous environment: The particle size effect. Cement and Concrete Composites. 133, 104655.
DOI: https://doi.org/10.1016/j.cemconcomp.2022.104655

[8] Chang, J., Xiong, C., Zhang, Y., et al., 2019. Foaming characteristics and microstructure of aerated steel slag block prepared by accelerated carbonation. Construction and Building Materials. 209, 222-233.
DOI: https://doi.org/10.1016/j.conbuildmat.2019.03.077

[9] Liu, S., Dou, Z., Zhang, S., et al., 2017. Effect of sodium hydroxide on the carbonation behavior of β-dicalcium silicate. Construction and Building Materials. 150, 591-594.
DOI: https://doi.org/10.1016/j.conbuildmat.2017.04.145

[10] Fang, Y., Chang, J., 2015. Microstructure changes of waste hydrated cement paste induced by accelerated carbonation. Construction and Building Materials. 76, 360-365.
DOI: https://doi.org/10.1016/j.conbuildmat.2014.12.017

[11] Li, W., Cao, M., Wang, D., et al., 2023. Improving the hydration activity and volume stability of the RO phases in steel slag by combining alkali and wet carbonation treatments. Cement and Concrete Research. 172, 107236.
DOI: https://doi.org/10.1016/j.cemconres.2023.107236

[12] Mo, L., Yang, S., Huang, B., et al., 2020. Preparation, microstructure and property of carbonated artificial steel slag aggregate used in concrete. Cement and Concrete Composites. 113, 103715.
DOI: https://doi.org/10.1016/j.cemconcomp.2020.103715

[13] Qu, M., Liu, P., Zhao, D., et al., 2020. CO_2 capture and conversion by an organosilane-modified cementitious material. Construction and Building Materials. 253, 119198.
DOI: https://doi.org/10.1016/j.conbuildmat.2020.119198

[14] Zajac, M., Skocek, J., Gołek, Ł., et al., 2023. Supplementary cementitious materials based on recycled concrete paste. Journal of Cleaner Production. 387, 135743.
DOI: https://doi.org/10.1016/j.jclepro.2022.135743

[15] Liu, P., Zhong, J., Zhang, M., et al., 2021. Effect of CO_2 treatment on the microstructure and properties of steel slag supplementary cementitous materials. Construction and Building Materials. 309, 125171.
DOI: https://doi.org/10.1016/j.conbuildmat.2021.125171

[16] Liu, P., Mo, L., Zhang, Z., 2023. Effects of carbonation degree on the hydration reactivity of steel slag in cement-based materials. Construction and Building Materials. 370, 130653.
DOI: https://doi.org/10.1016/j.conbuildmat.2023.130653

[17] Lu, B., Zhou, Y., Jiang, L., et al., 2024. High-purity vaterite $CaCO_3$ recovery through wet carbonation of magnesium slag and leaching residue utilization in cement. Cement and Concrete Composites. 145, 105353.

DOI: https://doi.org/10.1016/j.cemconcomp.2023.105353

[18] Liu, P., Zhang, M., Mo, L., et al., 2022. Probe into carbonation mechanism of steel slag via FIB-TEM: The roles of various mineral phases. Cement and Concrete Research. 162, 106991. DOI: https://doi.org/10.1016/j.cemconres.2022.106991

[19] Chang, J., Gu, Y., Ansari, W.S., 2020. Mechanism of blended steel slag mortar with CO_2 curing exposed to sulfate attack. Construction and Building Materials. 251, 118880. DOI: https://doi.org/10.1016/j.conbuildmat.2020.118880

[20] Mo, L., Zhang, F., Panesar, D.K., et al., 2017. Development of low-carbon cementitious materials via carbonating Portland cement-fly ash-magnesia blends under various curing scenarios: A comparative study. Journal of Cleaner Production. 163, 252-261. DOI: https://doi.org/10.1016/j.jclepro.2016.01.066

[21] Liu, S., Pan, C., Zhang, H., et al., 2023. Development of novel mineral admixtures for sulphoaluminate cement clinker: The effects of wet carbonation activated red mud. Journal of Building Engineering. 67, 105920. DOI: https://doi.org/10.1016/j.jobe.2023.105920

[22] Jiang, Y., Li, L., Lu, J.X., et al., 2022. Enhancing the microstructure and surface texture of recycled concrete fine aggregate via magnesium-modified carbonation. Cement and Concrete Research. 162, 106967. DOI: https://doi.org/10.1016/j.cemconres.2022.106967

[23] Zhang, W., Luan, Z., Ren, X., et al., 2022. Influence of alumina modulus on formation of high-magnesium clinker and morphological evolution of MgO. Cement and Concrete Research. 162, 106986. DOI: https://doi.org/10.1016/j.cemconres.2022.106986

[24] Mo, L., Panesar, D.K., 2012. Effects of accelerated carbonation on the microstructure of Portland cement pastes containing reactive MgO. Cement and Concrete Research. 42(6), 769-777. DOI: https://doi.org/10.1016/j.cemconres.2012.02.017

[25] Ye, J., Liu, S., Zhao, Y., et al., 2023. Development of ultrafine mineral admixture from magnesium slag and sequestration of CO_2. Buildings. 13(1), 204. DOI: https://doi.org/10.3390/buildings13010204

[26] Zhang, C., Liu, S., Tang, P., et al., 2023. Enhancing the hardening properties and microstructure of magnesium slag blocks by carbonation-hydration sequential curing. Journal of Building Engineering. 76, 107414. DOI: https://doi.org/10.1016/j.jobe.2023.107414

[27] Zhang, C., Liu, S., Luo, S., et al., 2022. Effects of sodium doping on carbonation behavior of α-CS. Cement and Concrete Composites. 131, 104607. DOI: https://doi.org/10.1016/j.cemconcomp.2022.104607

[28] Zhao, S., Liu, Z., Mu, Y., et al., 2020. Effect of chitosan on the carbonation behavior of γ-C2S. Cement and Concrete Composites. 111, 103637. DOI: https://doi.org/10.1016/j.cemconcomp.2020.103637

[29] Wang, D., Chang, J., 2019. Comparison on accelerated carbonation of β-C_2S, $Ca(OH)_2$, and C_4AF: Reaction degree, multi-properties, and products. Construction and Building Materials. 224, 336-347. DOI: https://doi.org/10.1016/j.conbuildmat.2019.07.056

[30] Mu, Y., Liu, Z., Wang, F., et al., 2018. Effect of barium doping on carbonation behavior of γ-C_2S. Journal of CO_2 Utilization. 27, 405-413. DOI: https://doi.org/10.1016/j.jcou.2018.08.018

[31] Mo, L., Hao, Y., Liu, Y., et al., 2019. Preparation of calcium carbonate binders via CO_2 activation of magnesium slag. Cement and Concrete Research. 121, 81-90. DOI: https://doi.org/10.1016/j.cemconres.2019.04.005

[32] Tan, Y., Liu, Z., Wang, F., 2022. Effect of tem-

perature on the carbonation behavior of γ-C_2S compacts. Cement and Concrete Composites. 133, 104652.
DOI: https://doi.org/10.1016/j.cemconcomp.2022.104652

[33] Luo, Z., Wang, Y., Yang, G., et al., 2021. Effect of curing temperature on carbonation behavior of steel slag compacts. Construction and Building Materials. 291, 123369.
DOI: https://doi.org/10.1016/j.conbuildmat.2021.123369

[34] Wasylenki, L.E., Dove, P.M., De Yoreo, J.J., 2005. Effects of temperature and transport conditions on calcite growth in the presence of Mg^{2+}: Implications for paleothermometry. Geochimica et Cosmochimica Acta. 69(17), 4227-4236.
DOI: https://doi.org/10.1016/j.gca.2005.04.006

[35] Xu, Z., Zhang, Z., Huang, J., et al., 2022. Effects of temperature, humidity and CO_2 concentration on carbonation of cement-based materials: A review. Construction and Building Materials. 346, 128399.
DOI: https://doi.org/10.1016/j.conbuildmat.2022.128399

[36] Liendo, F., Arduino, M., Deorsola, F.A., et al., 2022. Factors controlling and influencing polymorphism, morphology and size of calcium carbonate synthesized through the carbonation route: A review. Powder Technology. 398, 117050.
DOI: https://doi.org/10.1016/j.powtec.2021.117050

[37] Liu, S., Shen, Y., Wang, Y., et al., 2022. Upcycling sintering red mud waste for novel superfine composite mineral admixture and CO_2 sequestration. Cement and Concrete Composites. 129, 104497.
DOI: https://doi.org/10.1016/j.cemconcomp.2022.104497

[38] Li, H., Liu, Y., Yang, K., et al., 2022. Effects of synthetic CSH-tartaric acid nanocomposites on the properties of ordinary Portland cement. Cement and Concrete Composites. 129, 104466.
DOI: https://doi.org/10.1016/j.cemconcomp.2022.104466

[39] Xue, J., Liu, S., Ma, X., et al., 2022. Effect of different gypsum dosage on the chloride binding properties of C_4AF hydrated paste. Construction and Building Materials. 315, 125562.
DOI: https://doi.org/10.1016/j.conbuildmat.2021.125562

[40] Shen, P., Zhang, Y., Jiang, Y., et al., 2022. Phase assemblance evolution during wet carbonation of recycled concrete fines. Cement and Concrete Research. 154, 106733.
DOI: https://doi.org/10.1016/j.cemconres.2022.106733

[41] Liu, S., Shen, Y., Wang, Y., et al., 2021. Synergistic use of sodium bicarbonate and aluminum sulfate to enhance the hydration and hardening properties of Portland cement paste. Construction and Building Materials. 299, 124248.
DOI: https://doi.org/10.1016/j.conbuildmat.2021.124248

[42] Mao, Y., He, P., Drissi, S., et al., 2023. Effect of conditions on wet carbonation products of recycled cement paste powder. Cement and Concrete Composites. 144, 105307.
DOI: https://doi.org/10.1016/j.cemconcomp.2023.105307

[43] Shen, P., Lu, J., Zhang, Y., et al., 2022. Preparation aragonite whisker-rich materials by wet carbonation of cement: Towards yielding micro-fiber reinforced cement and sequestrating CO_2. Cement and Concrete Research. 159, 106891.
DOI: https://doi.org/10.1016/j.cemconres.2022.106891

BILINGUAL PUBLISHING GROUP

Journal of Building Material Science

https://journals.bilpubgroup.com/index.php/jbms

ARTICLE

Assessment and Rehabilitation of Damaged Buildings in Historic Benghazi City

***Vail Karakale*[1*], *Fathi M. Layas*[2], *Ramada E. Suleiman*[2]**

[1] *Department of Civil Engineering, Faculty of Engineering and Natural Sciences, Istanbul Medeniyet University, Istanbul, 34720, Turkey*

[2] *Department of Civil Engineering, Faculty of Engineering, University of Benghazi, PO Box 1308, Benghazi, Libya*

ABSTRACT

The primary focus of the study is to assess and classify the damage in the old Benghazi City. Specifically, it aims to evaluate buildings within a designated area, which is bordered by Umar Ibn Al-Aas Street to the south, Omar Al-Mukhtar Street to the north, Ben Issa Street to the east, and the extension of Gamal Abdel Nasser Street to the west. The main objective is to gather valuable insights and data that can support effective rehabilitation or reconstruction efforts. By comprehending the extent of the damage and categorizing it accordingly, the study seeks to provide essential information for decision-making processes and determine the most appropriate approach for restoration. The ultimate aim is to ensure the safe return of residents to the affected area. In addition to this, the restoration process aims to preserve and revitalize the city's religious, historical, and distinctive features. This includes safeguarding religious structures, landmarks, and elements that contribute to the city's unique identity. To achieve this, the study proposes separate rehabilitation schemes tailored for ordinary buildings and historic buildings.

Keywords: 3D Panels; Buildings; Rehabilitation; Historical buildings; Benghazi City

1. Introduction

The main goal of this study is to evaluate and categorize the damage in the old Benghazi City, which has suffered extensive destruction and is considered the most affected area within Benghazi. Specifically, the study focuses on assessing the region bounded

*CORRESPONDING AUTHOR:
Vail Karakale, Department of Civil Engineering, Faculty of Engineering and Natural Sciences, Istanbul Medeniyet University, Istanbul, 34720, Turkey; Email: vail.karakale@medeniyet.edu.tr

ARTICLE INFO
Received: 22 November 2023 | Revised: 12 December 2023 | Accepted: 25 December 2023 | Published Online: 30 December 2023
DOI: https://doi.org/10.30564/jbms.v5i2.6098

CITATION
Karakale, V., Layas, F.M., Suleiman, R.E., 2023. Assessment and Rehabilitation of Damaged Buildings in Historic Benghazi City. Journal of Building Material Science. 5(2): 51-59. DOI: https://doi.org/10.30564/jbms.v5i2.6098

COPYRIGHT
Copyright © 2023 by the author(s). Published by Bilingual Publishing Group. This is an open access article under the Creative Commons Attribution-NonCommercial 4.0 International (CC BY-NC 4.0) License. (https://creativecommons.org/licenses/by-nc/4.0/).

by Umar Ibn Al-Aas Street to the south, Omar Al-Mukhtar Street to the north, Ben Issa Street to the east, and the extension of Gamal Abdel Nasser Street to the west (**Figure 1**). The damage is classified into four distinct scenarios based on severity: minimum damage, medium damage (which is deemed rehabilitee), medium to high damage (requiring further study), and buildings that are completely demolished or set to be demolished. The evaluation aims to provide valuable insights and data that will support the effective rehabilitation or reconstruction of the targeted area. By comprehending the scope of the damage and categorizing it accordingly, the study seeks to guide decision-making processes and determine the most suitable course of action for restoration efforts. The ultimate objective is to ensure the safe return of residents to the damaged area. In addition to prioritizing the safety and well-being of the residents, the restoration process aims to preserve and revive the city's religious, historical, and unique features [1]. This entails reconstructing and repairing religious structures, historical landmarks, and other significant elements that contribute to the city's distinct identity. To achieve these objectives, the study proposes two rehabilitation approaches. For ordinary reinforced concrete (RC) buildings, the use of 3D panels is recommended [2,3]. This technique can facilitate the rehabilitation and reconstruction process. For historic buildings, a combination of textile reinforcements and special mortar is suggested. This approach ensures that the restoration maintains the original architectural style and materials, preserving the historical significance of these structures [4-7].

2. Criteria for classification of damage levels in the study

Table 1 provides an overview of the four damage level criteria employed to classify buildings within the study area. Additional information regarding these classifications can be found in sections 2.1 to 2.4.

2.1 Minimum damage or nill (L1)

In this section, the structure has either sustained no damage or only minor damage. It is generally considered to be in good condition and does not require any significant repairs or rehabilitation. Routine maintenance and regular inspections are typically sufficient to ensure its continued functionality and safety. Buildings that exhibit minimal damage are classified as having negligible damage. This includes micro-cracks with a width of less than 0.30 mm and a differential settlement of less than 3 cm. Additionally, the angular rotation of buildings in this category is less than 1/300. Negligible damage typically does not require extensive repairs or structural interventions.

Figure 1. Location of old Benghazi City on the general map.

Table 1. Criteria for classification of damage levels.

Damage level	Classification	Crack width (mm)	Angular rotation
L1	Minimum damage or nill	< 0.30	< 1/300
L2	Medium damage and can be rehabilitated	< 3	1/240 to 1/175
L3	Medium to high damage and needs thorough study	5-10	1/175 to 1/120
L4	Completely demolished or to be demolished	>10	1/120 to 1/70

2.2 Medium damage and can be rehabilitated (L2)

In this section, the structure has experienced moderate damage, which may affect its functionality or structural integrity to some extent. However, it is still deemed feasible to rehabilitate the structure through repairs and improvements. This usually involves assessing the extent of the damage, identifying the necessary remedial actions, and implementing appropriate repair strategies to restore the structure's performance and safety. Buildings categorized as having medium damage are those that still show signs of damage, even after the collapse of 1 or 2 structural elements, however, the damage is localized and still in the elastic range and can be recovered [8,9]. These buildings typically have cracks with a maximum width of 3 mm, experience a differential settlement ranging from 4-5 cm, and exhibit an angular rotation between 1/240 to 1/175. To address this damage, it is crucial to repair and seal both external and internal cracks using appropriate treatment materials and techniques. After the repairs, refinishing work is carried out in the damaged areas. Additionally, there may be a need to reinstall architectural elements, such as walls, doors and windows, once the necessary repairs have been completed.

2.3 Medium to high damage and the structure needs thorough study to decide on rehabilitation or demolition (L3)

In this section, the structure has suffered significant damage, ranging from moderate to high levels. The extent of the damage is substantial enough to warrant a comprehensive evaluation and study of the structure's condition [10]. Structural engineers and experts need to conduct detailed assessments, including structural analysis, material testing, and non-destructive inspections, to determine whether the structure can be effectively rehabilitated or if demolition is the more viable option. Based on the findings, a decision can be made on whether to proceed with rehabilitation efforts or to demolish the structure and rebuild it. Medium to high damage is observed after the collapse of one or more structural elements. It is characterized by cracks ranging from 5-10 mm in width or multiple cracks wider than 3 mm. The differential settlement typically ranges from 5-8 cm, and the angular rotation falls between 1/175 to 1/120. In this category, addressing the damage may involve opening, expanding, and cleaning the cracks before treating them with appropriate repair materials. If the building has brick walls, it may be necessary to replace some bricks and ensure proper refinishing of the walls. Windows and doors may be impacted, service pipes might break, and the effectiveness of insulation could be compromised.

2.4 Structure either completely demolished or to be demolished (L4)

In this section, the structure has either already been completely demolished, or it is determined that demolition is the only feasible course of action due to severe damage, safety concerns, or other factors. This decision is often made when the damage is extensive, compromising the structural integrity to such an extent that rehabilitation is no longer practical or cost-effective. Demolition involves the controlled dismantling or destruction of the structure, making way for potential reconstruction or repurposing of the site. In this case, the collapse of multiple structural elements. It is evident through the presence of large cracks > 10 mm in width. The walls may exhibit significant curvature or even collapse entirely, while the floors could show noticeable slopes or complete failure. Additionally, door and window frames may be visibly distorted. Low-stiffness beams may also be observed in severe damage scenarios. The differential settlement in such cases ranges from 8-13 cm, and the angular rotation falls between 1/120 to 1/70.

3. Results of visual inspection and classification: Assessing damage levels

A rigorous on-site examination was conducted

on a substantial number of buildings in the region. These buildings were subsequently classified and evaluated based on the expertise and familiarity of the research participants with the area. A comprehensive inspection was conducted on a total of 300 buildings, which consisted of 80 structures dating back to the Italian colonial era and 220 units constructed in subsequent periods. The findings of the evaluation are presented in **Table 2**.

Table 2. Classification of building damage extent.

Damage level	No. of buildings	% of total
L1	168	56%
L2	83	27%
L3	13	4%
L4	36	13%
Total	300	100%

3.1 Buildings without significant damage

Among the buildings inspected, a subset of 168 structures (56% of the total) fall into this category. The observed damage in these buildings is non or limited to specific architectural elements while maintaining the integrity of their structural components. Examples of these buildings are shown in **Figure 2**.

Figure 2. Examples illustrating buildings without significant damage.

3.2 Buildings with medium damage: Feasibility of rehabilitation

Within the set of examined structures, a subset of 83 buildings, accounting for 27% of the total, have been identified as having medium damage. These buildings display a level of damage that is deemed feasible for rehabilitation to their structural integrity. This rehabilitation process will involve the implementation of appropriate repair techniques, the use of suitable materials, and the application of structural reinforcements where necessary. Illustrative examples are the buildings shown in **Figure 3**.

Figure 3. Examples illustrating buildings with medium damage.

3.3 Damaged buildings requiring further investigation

Within the examined structures, a subset of 13 buildings (4%) necessitates additional studies that involve testing the structural elements and conducting a comprehensive structural analysis. These investigations are crucial for making informed decisions regarding whether to rehabilitate or proceed with demolition and subsequent reconstruction. Illustrative examples are the buildings shown in **Figure 4**.

3.4 Completely demolished or severely damaged buildings

Out of the inspected buildings, a total of 36 structures (13%) were found to be either completely collapsed or severely damaged. These buildings are determined to be beyond repair and necessitate dem-

olition, followed by the reconstruction process. Illustrative examples are the buildings shown in **Figure 5**.

Figure 4. Examples illustrating buildings require further investigation.

Figure 5. Examples illustrating buildings of completely demolished or severely damaged.

4. Historical buildings in old Benghazi City

A significant proportion of the buildings in this area hold historical importance, primarily dating back to the Italian colonial era. These buildings, with their rich heritage and architectural fabric, are recommended for rehabilitation to ensure the preservation of their historical status. To maintain the cultural value of these historical buildings, it is advised to undertake their rehabilitation using the same architectural style and materials that were originally employed in their construction. This approach not only safeguards their historical integrity but also contributes to the preservation of the overall architectural fabric of the area. Illustrative examples are the buildings shown in **Figure 6**.

Figure 6. Examples illustrating old structure buildings.

These buildings hold significant historical value within the study area, they are located as shown in **Figure 7**. Photos of the buildings are shown in **Figure 8**. Each building represents a distinct aspect of the region's heritage and cultural identity. Preserving these special buildings is crucial to maintaining the historical fabric and upholding the architectural legacy of the area. These buildings are:

1) Old Mosque
2) Osman Mosque
3) The Cathedral Church
4) Qasr Al-Manar (University of Libya)
5) The Italian Consulate

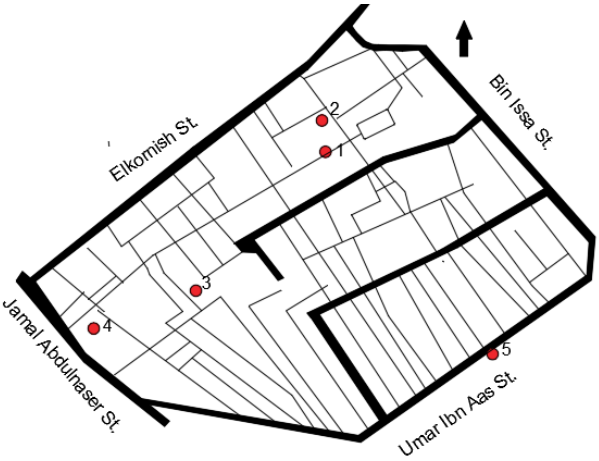

1. Old Mosque

2. Osman Mosque

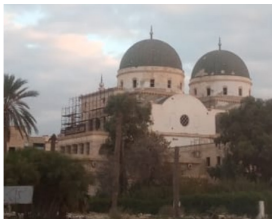

3. The Cathedral Church

4. Qasr Al-Manar

5. The Italian Consul

Figure 8. Photos of prominent historical buildings.

5. Rehabilitation materials and techniques

5.1 Rehabilitation of reinforced concrete frame buildings with 3D panels

3D panels, also known as three-dimensional panels or sandwich panels, are prefabricated building components that consist of a lightweight core material (such as foam, polystyrene or honeycomb) sandwiched between two layers of structural material (such as concrete or mortar). These panels are designed to provide strength, rigidity, and insulation to structures. In the context of rehabilitating reinforced concrete frame buildings, 3D panels can offer several advantages:

1) **Strengthening and structural integrity**: By installing 3D panels on the existing concrete frame, the panels can provide additional strength and enhance the structural integrity of the building. This is particularly useful in cases where the original concrete elements have deteriorated or become weak over time.

2) **Seismic resistance**: Reinforced concrete frame buildings are often vulnerable to seismic forces. The use of 3D panels can improve the seismic resistance of the structure by adding stiffness and reducing the chances of structural failure during an earthquake.

3) **Thermal insulation**: 3D panels typically have good insulation properties, which can help improve the energy efficiency of the rehabilitated building. By reducing heat transfer through the walls, the panels can contribute to maintaining a comfortable indoor environment and potentially reducing heating and cooling costs.

4) **Acoustic insulation**: Depending on the composition of the 3D panels, they can also provide soundproofing benefits. This can be advantageous in urban areas or buildings located near noisy environments, as it helps to minimize the transmission of external noise into the interior spaces.

5) **Speed of construction**: Prefabricated 3D panels are manufactured off-site, allowing for faster construction compared to traditional on-site methods. This can significantly reduce the overall project duration and minimize disruption to building occupants during the rehabilitation process. It's important to note that the use of 3D panels for rehabilitating reinforced concrete frame buildings should be done in consultation with structural engineers and professionals experienced in retrofitting techniques. Each building is unique, and proper analysis and design are necessary to ensure that the panels are appropriately integrated and meet the specific requirements and safety standards. The use of 3D panels can be a viable option for rehabilitating reinforced concrete frame buildings, offering benefits such as enhanced structural strength, improved seismic resistance, thermal and acoustic insulation, and faster construction. **Figures 9 and 10** show the details and materials used in this system.

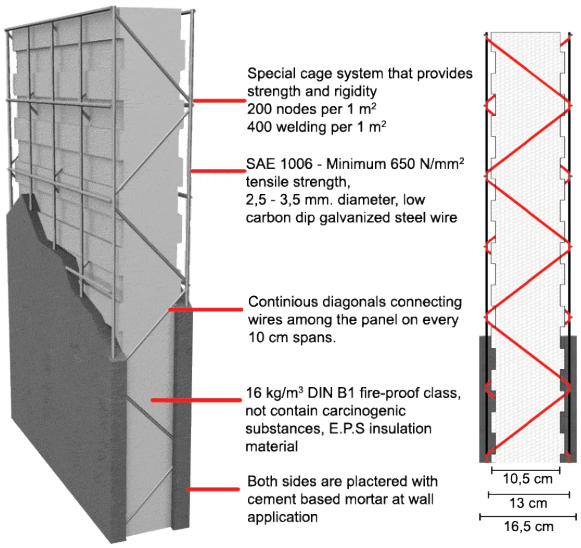

Figure 9. 3D view and cross-section details of the 3D panel.

5.2 Restoring historical buildings: Utilizing textile reinforcements and special mortars

The repair and rehabilitation of old historic structures is a complex task that requires careful consideration of the interaction between existing and new elements. Unfortunately, there is often a lack of global technical guidelines for such projects, which can make the process challenging. However, there are certain techniques and materials that are commonly

employed in the restoration of historic structures, particularly in places like old Benghazi city. One approach involves the use of textile reinforcements and lime-based mortars. Textile reinforcements, such as fibers or fabrics, are incorporated into the mortar to improve its mechanical properties and increase its resistance to cracking and deformation. Lime-based mortars, on the other hand, are preferred over cement-based mortars due to their breathable and flexible properties, which are well-suited for historical structures that are susceptible to decay and deterioration. In the restoration of historic structures, lime-based mortars are often modified by incorporating various additives to enhance their performance [4,5]. Some commonly used additives include white cement, gypsum, lignin sulfonate, and silica fume. These additives can impart specific properties to the mortar, making it more suitable for restoration work. For example, the addition of silica fume to lime-based mortars has been shown to improve their mechanical strength. Silica fume is a byproduct of the silicon and ferrosilicon alloy production process and is composed of very fine particles. When added to lime mortar, it enhances the mortar's compressive, tensile, and shear strengths, making it more robust and durable. On the other hand, the inclusion of lignin sulfonate in lime-based mortars can improve their performance during wetting and drying cycles. Lignin sulfonate is a byproduct of the pulp and paper industry and acts as a water-reducing and plasticizing agent. It enhances the workability and cohesion of the mortar and reduces the detrimental effects of moisture variations on its durability. This is particularly important for historic structures that may be exposed to fluctuating moisture levels. In terms of structural behavior and bonding, lime-based mortars with lignin sulfonate have been found to exhibit improved load capacity. This means that they are better able to withstand external forces and maintain their structural integrity. These mortars can be used to reinforce model walls, providing strength and stability to the structure. **Figure 11** illustrates restoration work carried out on a historic structure, demonstrating how the application of these materials can help preserve and protect the building while maintaining its historical character. The utilization of lime-based mortars with additives, such as silica fume and lignin sulfonate, is gaining popularity in the restoration of heritage buildings. These mortars offer favorable mechanical properties, durability during wetting and drying cycles, and improved load capacity for structural behavior and bonding. Their breathable and flexible nature makes them well-suited for historic structures prone to decay and deterioration, ensuring their long-term preservation.

Figure 10. Use 3D panels as infill walls with good connections with the peripheral frames.

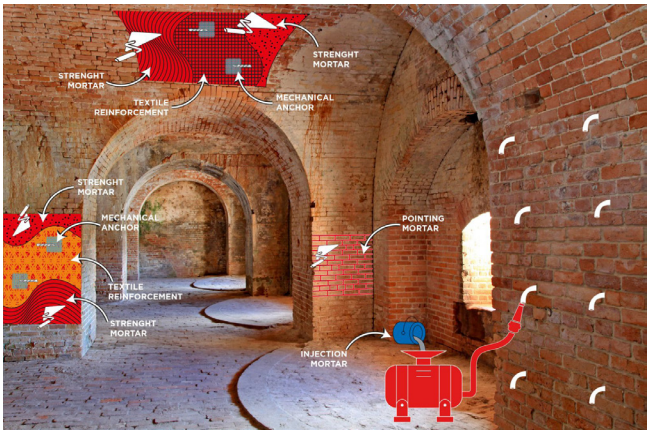

Figure 11. Rehabilitation with textile reinforcements and special mortars.

6. Conclusions

In this study, the authors conducted an assessment specifically focused on evaluating and categorizing

the damage in the old area of Benghazi City. The aim was to gain a better understanding of the condition of buildings within a designated region and provide insights for rehabilitation and reconstruction efforts. The researchers performed visual inspections of over 300 building units. These inspections involved carefully examining the structures to identify and document any visible damage or deterioration. In addition, more than 100 photographs were captured to supplement the visual inspection process and provide a visual record of the damage observed. The main objective of the study was to classify the damage into four levels based on its severity so that decision-makers can prioritize and plan for appropriate restoration and rehabilitation strategies. The study also proposed specific methods for restoring the damaged buildings. One approach suggested the use of 3D panels for reinforced concrete frame buildings. These panels can provide structural reinforcement and contribute to the overall stability and safety of the buildings. Additionally, the researchers recommended employing textile reinforcements with special mortars for historical structures. This approach can help preserve the unique architectural characteristics of the historic buildings while ensuring their structural integrity.

Author Contributions

The three authors equally, contributed to this research.

Conflict of Interest

There is no conflict of interest.

References

[1] El-Agouri, F.A., Karakale, V., 2018. Privacy regulation, spatial culture and communities in a communally diverse city: Ghadames, Libya. Journal of World Architecture. 2(1).
DOI: https://doi.org/10.26689/jwa.v2i1.516

[2] Mowrtage, W., 2012. Low-rise 3D panel structures for hot regions: design guidelines and case studies. Arabian Journal for Science and Engineering. 37(3), 587-600.
DOI: https://doi.org/10.1007/s13369-012-0204-7

[3] Mowrtage, W., Karadogan, F., 2008. Behavior of single-story lightweight panel building under lateral loads. Journal of Earthquake Engineering. 13(1), 100-107.
DOI: https://doi.org/10.1080/13632460802347380

[4] Stempniewski, L., Mowrtage, W., Urban, M., 2014. Seismic collapse prevention of non-structural infill masonry using eq-top: An easy earthquake fibre retrofitting system. Arabian Journal for Science and Engineering. 39, 1599-1605.
DOI: https://doi.org/10.1007/s13369-013-0793-9

[5] Abdel-Mooty, M., Khedr, S., Mahfouz, T., 2009. Evaluation of lime mortars for the repair of historic buildings. WIT Press: Wessex, UK.

[6] Karakale, V., 2018. Restoration of an Ottoman historical building in Istanbul. Journal of World Architecture. 2(1).
DOI: https://doi.org/10.26689/jwa.v2i1.515

[7] Karakale, V., 2017. Use of structural steel frames for structural restoration of URM historical buildings in seismic areas. Journal of Earthquake and Tsunami. 11(4), 1750012.
DOI: https://doi.org/10.1142/S1793431117500129

[8] Layas, F.M., Karakale, V., Suleiman, R.E., 2023. Behavior of RC buildings under blast loading: Case study. Recent Progress in Materials. 5(3), 1-12.
DOI: https://doi.org/10.21926/rpm.2303029

[9] Karakale, V., Suleiman, R.E., Layas, F.M., 2023. Lateral load behavior of RC buildings exposed to fire: Case study. Journal of Asian Architecture and Building Engineering. 22(1), 274-285.
DOI: https://doi.org/10.1080/13467581.2022.2026777

[10] Karakale, V., Özgür, E., Ataoğlu, Ş., 2023. Site observations on buildings' performance in Hatay Province after Kahramanmaraş earthquakes. El-Cezeri. 10(3), 506-516.
DOI: https://doi.org/10.31202/ecjse.1253284

[11] Karadogan, F., Pala, S., Ilki, A., et al., 2009. Improved infill walls and rehabilitation of existing low-rise buildings. Seismic risk assessment and retrofitting: With special emphasis on existing low-rise structures. Springer: Dordrecht. pp. 387-426.
DOI: https://doi.org/10.1007/978-90-481-2681-1_19

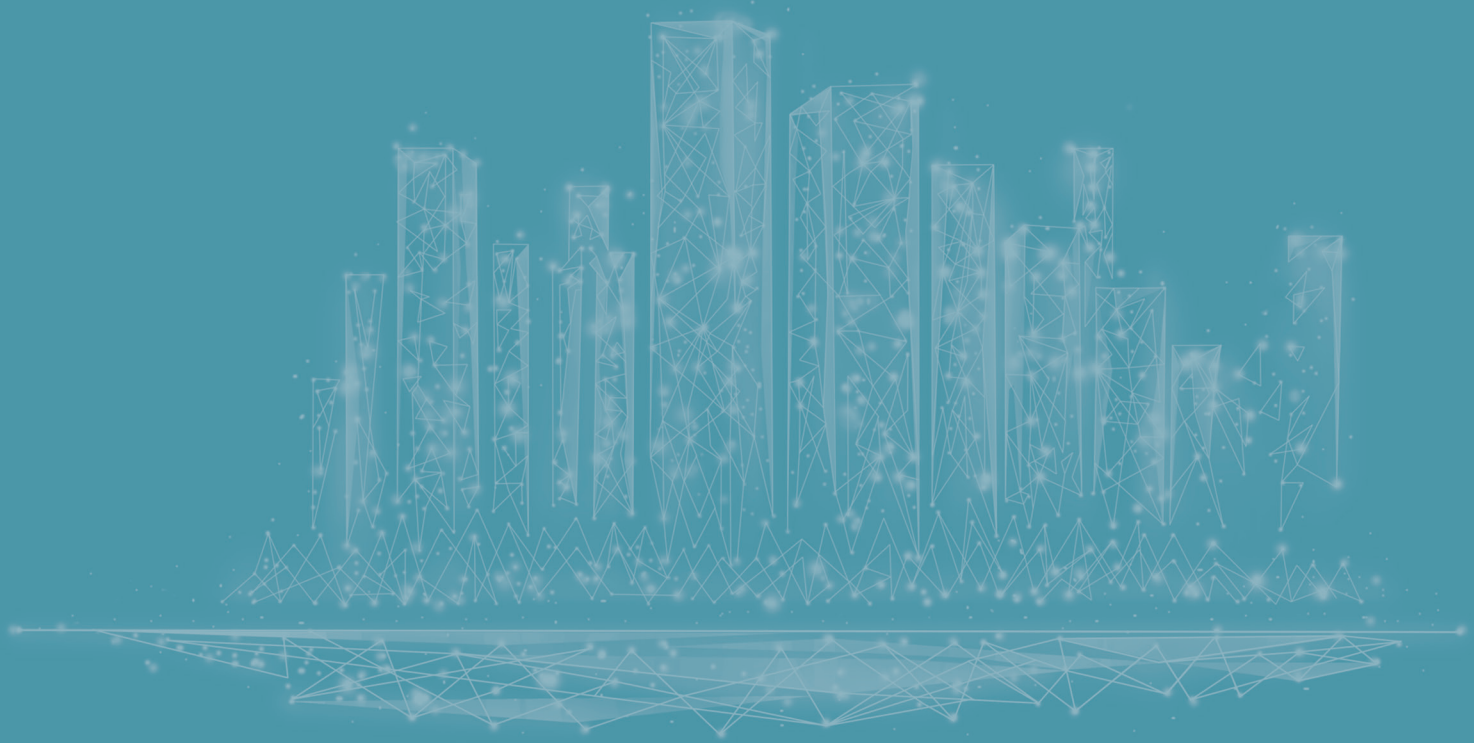

BILINGUAL
PUBLISHING
GROUP

Tel:+65 65881289
E-mail: contact@bilpublishing.com
Website:https://journals.bilpubgroup.com

2630-5216
02
9 772630 521231